

**TRI-HP
PROJECT**

Trigeneration systems based on
heat pumps with natural refrigerants
and multiple renewable sources

Investigation of coatings and metallic materials for icephobic properties

Deliverable number: D3.5

Version 1.0



Funded by the European Union's Horizon 2020 research and innovation programme under grant agreement N. 814888. The sole responsibility for the content of this paper lies with the authors. It does not necessarily reflect the opinion of the European Commission (EC). The EC is not responsible for any use that may be made of the information it contains.

This page is intentionally left blank

Project Acronym:	TRI-HP
Project URL:	http://www.tri-hp.eu
Responsible partner:	DTI
Deliverable nature:	Report (R)
Dissemination level:	Public (PU)
Contractual Delivery Date:	December 31, 2020
Actual Delivery Date	January 4, 2021
Number of pages:	41
Keywords:	Economic assessment
Authors:	Jens Frandsen (DTI), Olivier Schmid (IKKU), Maïke Schubert(SPF), Ricardo Losada (DTI)
Collaborators:	Joerg Brand (ILAG), Daniel Carbonell (SPF-HSR), Olga Santos (ALFA LAVAL)
Review:	Daniel Carbonell (SPF-HSR)
Approval:	Daniel Carbonell (SPF-HSR)

Revision History

Date	Version	Changes
January 4, 2021	v1.0	1 st version submitted to EC

TRI-HP CONSORTIUM

 INSTITUT FÜR SOLARTECHNIK	Oberseestrasse 10 CH-8640 Rapperswil, Switzerland	Coordinator : Dr. Daniel Carbonell Dani.Carbonell@spf.ch
 Inspiring Business	Área Anardi, 5. E-20730 Azpeitia (Gipuzkoa), Spain	Mr. Andoni Diaz de Mendibil andoni.diazdemendibil@tecnalia.com
	Murtenstrasse 116, CH-3202, Frauenkappelen, Switzerland	Mr. Raphael Gerber raphael.gerber@cadena.ch
 Shaping Energy for a Sustainable Future	Jardins de les Dones de Negre 1 2 ^a pl. 08930 Sant Adrià de Besòs (Barcelona)	Dr. Jaume Salom jsalom@irec.cat
	Box 74, 22100 Lund, Sweden	Mr. Mats Nilsson MatsR.Nilsson@alfalaval.com
 swiss quality coatings	Hämmerli 1, CH-8855, Wangen, Switzerland	Mrs. Stephanie Raisch stephanie.raisch@ilag.ch
Institut für sozial-ökologische Forschung 	Hamburger Allee 45, Frankfurt am Main, 60486, Germany	Dr. Immanuel Stiess stiess@isoe.de
 Norwegian University of Science and Technology	Kolbjørn Hejes vei 1D (B249), No-034 Trondheim, Norway	Dr. Alireza Zendejboudi alireza.zendejboudi@ntnu.no
	Kongsvang Allé 29, 8000 Aarhus C, Denmark	Mr. Claus Bischoff clb@teknologisk.dk
 Hochschule Karlsruhe Technik und Wirtschaft UNIVERSITY OF APPLIED SCIENCES Institute of Refrigeration, Air-Conditioning and Environmental Engineering	Moltkestr. 30, 76133 Karlsruhe, Germany	Dr. Prof. Michael Kauffeld Michael.Kauffeld@hs-karlsruhe.de
 Federation of European Heating, Ventilation and Air Conditioning Associations	Rue Washington 40, 1050 Brussels, Belgium	Ms. Anita Derjanecz ad@rehva.eu
 EQUIPOS FRIGORIFICOS COMPACTOS,S.L.	C/Zuaznabar 8 Pol. Ind. Ugaldetxo, Oiartzun, 20180, Spain	Mr. Gabriel Cruz g.cruz@equiposfrigorificoscompactos.com

CONTENTS

1	Introduction	2
2	Technological solutions to avoid/prevent ice blockage proposed in TRI-HP	3
2.1	Coatings	3
2.1.1	DTI Coatings	4
2.1.2	ILAG coatings	4
2.2	Bulk Materials	7
3	Small scale laboratory testing	10
3.1	Coatings: Laboratory tests	10
3.1.1	Results and Discussion	13
3.2	Amorphous metallic materials: Laboratory tests	19
3.2.1	Basic screening method	19
3.2.2	Advanced screening method	20
3.2.3	Discussion	24
4	Large scale testing	25
4.1	Coatings: Large scale testing	25
4.1.1	Experimental test setup for coated tubes at SPF	25
4.1.2	Results of tube tests with water flows	27
4.1.3	Discussion	28
4.2	Large scale testing of amorphous metallic surfaces	30
4.2.1	Experimental setup at UASKA	30
4.2.2	Results of brand strip materials	33
4.2.3	Results of electroless nickel treated tubes	35
4.2.4	Conclusion	37
5	Conclusion	38

EXECUTIVE SUMMARY

This report summarizes the results of the activities related to coatings and metallic materials with icephobic or ice depressing capabilities within the H2020 European project “TRI-HP”. The overall goal of the TRI-HP project is the development of trigeneration systems based on electrically driven natural refrigerant heat pumps coupled with renewable electricity generators (PV). The systems are aiming to provide heating, cooling and electricity to multi-family residential buildings with a self-consumed renewable share of 80 %. One of the systems developed is based on a supercooling ice slurry heat pump. A successful development of such a system relies on the development of a heat exchanger that can supercool water to temperatures around $-2\text{ }^{\circ}\text{C}$ to $-3\text{ }^{\circ}\text{C}$ without forming ice, the so-called supercooler. This report summarizes the development and testing results of surfaces and materials to produce these supercoolers.

In order to achieve the goals of the proposed activities different technological solutions based on metallic materials, surface treatments and coatings have been developed and tested. These solutions aim to improve the performance of supercooling heat exchangers by avoiding the nucleation of ice on the surface of the supercooling heat exchanger and preventing its blockage.

Three main targets were defined at the initial stage: first, development of coatings for preventing/delaying ice formation that could be applied on already existing heat exchangers (supercoolers); second, to identify bulk material for preventing/delaying ice formation to be used for constructing new heat exchangers (supercoolers); third, to validate the icephobic functionality of coatings and bulk materials for continuous supercooled water flows.

Regarding the required icephobic performance, the focus was the ability of the new coatings and materials to lower the freezing temperature (freeze depression). Ideally, the TRI-HP solutions should enable a stable subcooling degree of 2-3 K.

Icephobic coatings

Two main ideas for coatings to prevent the formation of ice that have been used: i) hydrophobic coatings, i.e. water repellent surfaces; ii) amphiphilic coatings, hydrophobic surfaces that expose some hydrophilic functional groups that can be classified as water structure breakers. In total, 18 coatings prepared by DTI (13 hydrophobic and 5 amphiphilic) and 8 coatings prepared by ILAG were tested. To assess the coatings anti-ice properties, custom-made tests and equipment was developed. With this it was possible to test coatings in both atmospheric and submerged conditions of surfaces with an area of 25 cm^2 without water flows. Moreover, a method to test shear stress ice adhesion was developed. Low ice adhesion could have an impact on facilitating the ice removal when using high mass flows in the supercoolers. Even though many different chemical families were tested there were no clear trend when comparing them. Hydrophobic siloxanes based coatings performed well across all tests, but even among those, there were differences which could not be correlated to surface energy or contact angle measurements, indicating that other factors may have impact as well.

In the small-scale laboratory tests, five of the hydrophobic systems demonstrated good water stability and potential to achieve a stable supercooling of 3 K compared to uncoated references. Another positive effect has been observed for some coatings (specially the amphiphilic systems), which is their ability to lower the ice adhesion down to less than 30 kPa (ultra-low ice adhesion), which may be of great interest for easy removal of ice.

Even though many different chemical families were tested no clear trends were found when comparing them. Hydrophobic siloxanes based coatings performed well across all tests, but even among those, there were dif-

ferences which could not be correlated to surface energy or contact angle measurements, indicating that other factors may have impact as well.

Despite the very good results with surfaces of around 25 cm^2 without water flows, the large-scale laboratory results with surfaces around 0.3 m^2 and with water flows conducted at SPF showed less benefits in terms of ice depression compared to stainless steel. Differences between coatings and stainless steel were significant at water velocities of 0.2 m/s , but reduced for water velocities of around 0.5 m/s . However, all coatings performed significantly better compared to a rough copper surface with small defects. This could bring significant improvements in corrugated flat plates heat exchangers where the brazing would lead to non-smooth surfaces. Results of heat exchangers (supercoolers) using the best coatings will be available in spring of year 2021.

Amorphous metallic materials

The idea behind the use of amorphous metallic materials is based on the theory of crystal growth. In order to form a solid crystal lattice in a liquid surrounding enough molecules have to come together to exceed an energy barrier, which is called free surface energy. This energy barrier is what makes supercooling possible in the first place. Therefore, the approach is to increase this energy barrier by introducing stresses within the water molecules. This is achieved by bringing the water into contact only with materials that have a different crystal structure. The supercooled water molecules striving to form a hexagonal ice crystal to which other molecules can attach after its formation. The use of amorphous materials, according to our theoretical approach, creates a mismatch of surface near water molecules to the solid surface of the heat exchanger and thus tensions.

A total of 12 materials were investigated (10 amorphous and 2 nanocrystalline). The samples consist of high-alloy band strips which are usually used as capacitor material in high-performance electronics. A small-scale laboratory test at UASKA showed that all the proposed materials provide more reliable supercooling performance compared to the face-centered cubic crystal structure of copper and aluminum. An advanced contact angle measurement was conducted where the freezing process was investigated by a digital microscope. It was expected that the contact angle changes right before the freezing suddenly starts, which would be an additional indicator for a promising material. Unfortunately this method did not work out for that purpose. The materials for the flow test were then selected based only on their freeze depression and freeze delay results. When the results were analyzed, it was found that nickel was present in the alloys that performed best. This led to the new approach of a high phosphorous nickel plating, which also forms an amorphous surface. This method is also cheaper and easier to apply to the heat exchanger surface.

In the experiment with water flows the amorphous metallic band strips were placed in a special designed heat exchanger with a surface of 0.04 m^2 for each channel. However, their ability to delay freezing of amorphous metallic materials could not be demonstrated in this experiment. Freezing started at insignificant supercooled temperatures, so no reliable statement can be made about freeze suppression. The testing method employed for the band strip materials had a drawback. The dimension of a heat exchanger was limited to the size of the band strip which led to a low heat transfer surface which was too low to supercool water significantly. Moreover, in all tests it was found that a sharp edge was a starting point for the freezing difficulting the comparison between materials. Regarding the amorphous metallic materials it was found that a long term water exposure led to corrosion of those containing iron.

As a second approach, copper tubes were treated by the electroless nickel plating method and installed in a tube and shell heat exchanger. The nickel tubes with a total surface area of around 0.13 m^2 were mounted inside a shell. The water was supercooled inside the tubes while brine was flowing counterflow in the shell of the heat exchanger. When compared to copper tubes, the outlet temperature achieved was lower compared to the copper

tubes. It is therefore expected that high phosphorous nickel plating has advantageous properties for the use in supercoolers. This approach will be tested in real heat exchanger (supercoolers) and will be presented in spring of year 2021.

LIST OF ACRONYMS

CFD	Computational Fluid Dynamics
TRL	Technological Readiness Level
DFT	Dry Film Thickness
SCA	Static Contact Angle
Adv. CA	Advancing Contact Angle
Rec. CA	Receding Contact Angle
CAH	Contact Angle Hysteresis
SE	Surface Energy
Ra	arithmetic average roughness value
Rz	average peak-to-valley height
θ_Y	Young's contact angle
ΔG_S	Change of free surface energy
ΔG	Change of Gibbs energy
ΔG_V	Change of free volume energy

1 INTRODUCTION

The TRI-HP project focuses on development and demonstration in the laboratory of trigeneration¹ system to will supply heating, cooling and electricity with high share on on-site renewables. The systems are based on natural refrigerant heat pumps coupled with PV and make use of different renewable heat sources for the heat pump. On of those sources is the use of solar energy combined with an intermediate ice storage.

In the TRI-HP system ice-slurry, that is defined as a mixture of ice particles finely dispersed in water, is used as an energy storage medium and produced by the supercooling method. In this method, a stream of water which is flowing into a heat exchanger (supercooler) is cooled by a few degrees below normal freezing point. Upon leaving the evaporator, the supercooled water flow is physically disturbed in a crystallizer to generate ice crystals, see Fig. 1.1. The main advantage of the supercooling method for ice slurry production is the use of known technology without extra energy to operate. However, the heat exchanger for supercooling must ensure that there is no crystallization happening inside, otherwise, the slurry generation may stop due to its blockage. The best way to realize the continuous ice generation with supercooling water is to find an effective way to prevent the nucleation of ice on the surface of the supercooling heat exchanger. Different technological solutions, based on icephobic coatings and bulk materials have been studied. The goal is to improve the efficiency of the supercooler for producing ice-slurry by preventing or delaying the formation of ice. The ice fraction in the ice slurry depends on the supercooling of the liquid leaving the evaporator (supercooler) and increases by approximately 1.25 % per °C. In TRI-HP, the goal was to develop surfaces able to achieve a stable supercooling of 3 K to 4 K which would remain ice-free.

This document summarizes the results obtained including the main conclusions the potentials of these solutions and pending development needed for deployment.

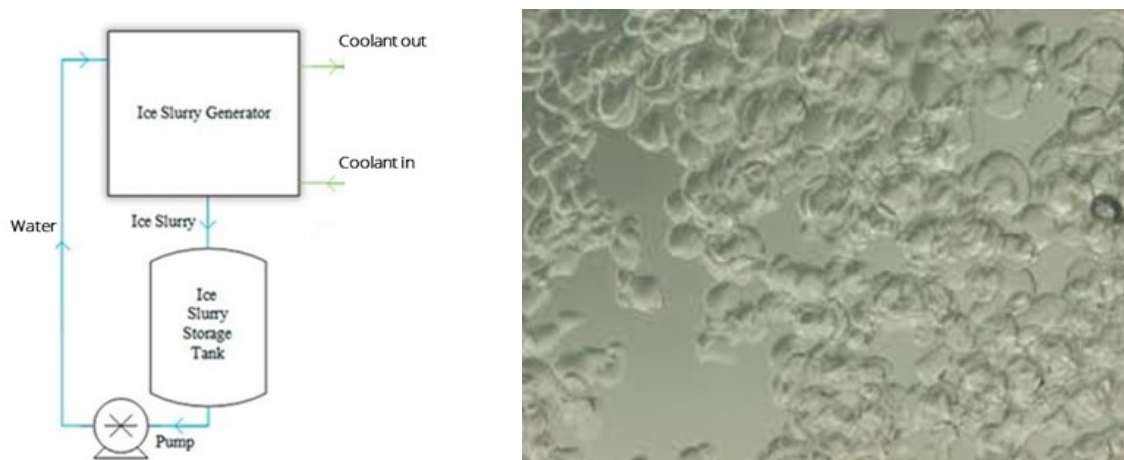


Figure 1.1: Left: Ice slurry production by the supercooling method. Right: ice slurry (Wikipedia).

¹tri stands for heating, cooling and electricity

2 TECHNOLOGICAL SOLUTIONS TO AVOID/PREVENT ICE BLOCKAGE PROPOSED IN TRI-HP

To achieve the goals of the project, two different approaches have been followed; a) the application of icephobic coatings on the surface of the supercoolers (already existing heat exchangers) and b) the fabrication of new supercooling heat exchangers from bulk materials with ice inhibiting properties.

Initial laboratory tests at small-scale were done to evaluate the icephobic properties of coatings and bulk materials. For coatings, the following parameters were evaluated; *Freeze depression* which is the ability of coatings to lower the freezing temperature, *freezing delay* which is the capacity of coatings to delay the formation of ice at a particular temperature, and the ice adhesion that is the adhesion strength of ice to particular surfaces. In the case of the bulk materials, the main characterization technique at small-scale was the evaluation of the freeze depression properties.

After the initial laboratory screening, the best performing coatings and bulk materials were tested in a custom-made large-scale laboratory test rigs at SPF (coatings) and UASKA (bulk materials) with water flows. This experimental test proof the use of supercooling in a laboratory bringing the solutions to TRL 4. Thanks to this activity a selection of materials and coatings to be applied on industrially relevant supercoolers was possible. These kind of test represent a step in between the tests at sample level without water flows and the experiments with industrially relevant supercoolers that would bring the solution to TRL 5 for residential heat pumps.

2.1 COATINGS

DTI and ILAG followed different strategies to fabricate the icephobic coatings that have been analyzed in the project. DTI focused on organic-inorganic hybrid and silicon rubber derived coatings to generate hydrophobic and amphiphilic surfaces. ILAG approach was based on organic-inorganic and organic coatings with hydrophobic properties.

The coatings were tested on different substrate materials, aluminum and copper. Aluminum was used as reference material to evaluate the icephobic properties. Application test had been carried out in copper since the supercoolers for the TRI-HP systems are expected to be copper-brazed plate heat exchangers.

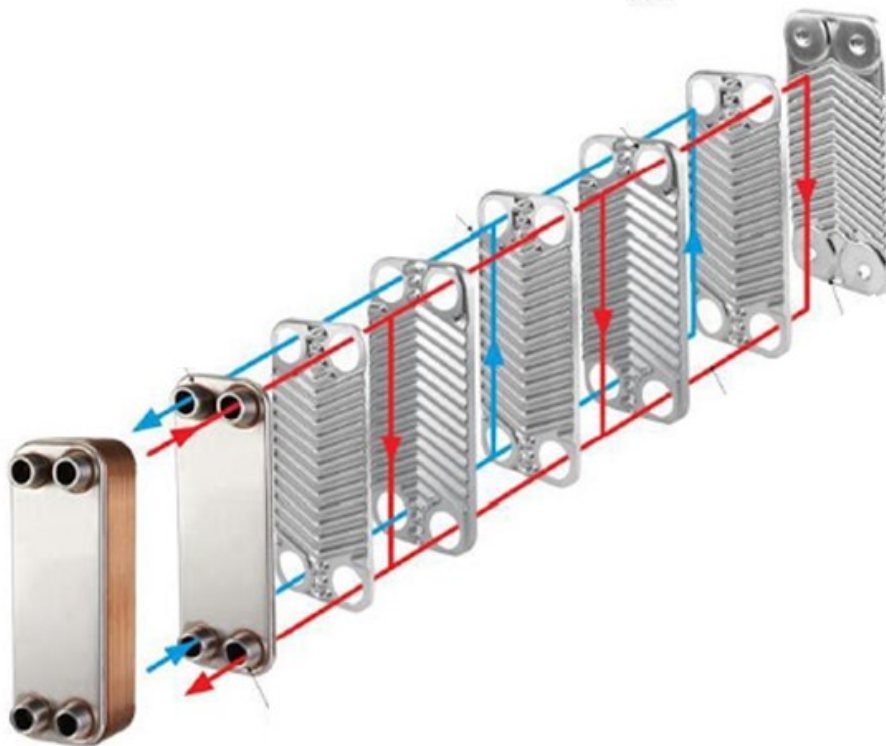


Figure 2.1: Scheme copper-braze plate heat exchanger

2.1.1 DTI Coatings

The organic-inorganic hybrid coatings were either prepared by sol-gel processing or via moisture-curing route. The precursor's solutions were prepared from organosilanes and additional organic precursors.

DTI investigated several hydrophobic and amphiphilic organic-inorganic hybrid coatings, most of them based on existing recipes or variations thereof. The hydrophobic coatings were seen as promising due to previously demonstrated high water repellence, low film thickness in the range of a few μm (<15) and high stability. Furthermore, those coatings were previously applied against frost spreading [1]. Regarding the amphiphilic coatings, they were fabricated using similar strategies to the hydrophobic coatings, but they were modified by specific hydrophilic additives to create the amphiphilic surfaces. Amphiphilicity is commonly used to enhance the biofouling resistance of surfaces but has been also reported as a strategy to generate icephobic surfaces with low ice adhesion [2].

2.1.2 ILAG coatings

ILAG has used 4 different strategies to fabricate hydrophobic coatings which have shown icephobic properties in preliminary tests. The dry film thickness (DFT) was optimized to enhance mechanical resistance, while still having good thermal conductivity. ILAG coatings are based on Fluoropolymer, Polysiloxane, and Fluoroethylenevinylether containing coatings. Target DFT for these systems is approx. 10 μm to 25 μm where some contain a bonding agent for better copper adhesion.

In total 8 hydrophobic coatings from ILAG and 18 DTI coatings (13 hydrophobic and 5 amphiphilic) were included in the testing phase. Besides, for benchmarking purposes other organic commercial coatings were included in the experimental campaign. In Table 2.1, an overview of the coatings tested and their general properties, including Static Contact Angle (SCA), Advancing Contact Angle (Adv. CA), Receding Contact Angle (Rec. CA), Contact Angle Hysteresis (CAH), Surface Energy (SE) and thickness.

Coating	SCA [°]	Adv CA [°]	Rec CA [°]	CAH [°]	SE [mN m ⁻¹]	Thickness [μm]
<i>Metal references*</i>						
Alu plate	92.6 ± 1.5	92.4 ± 2.5	55.8 ± 3.1	36.6	~58	-
<i>DTI-Coatings (hydrophobic)*</i>						
DTI-01	104.2 ± 1.1	104.3 ± 1.5	91.3 ± 1.1	13.0	20-22	13.48 ± 2.30
DTI-02 ****	87.6 ± 1.0	88.8 ± 1.8	72.9 ± 0.7	15.9	24-25	11.06 ± 2.30
DTI-03	104.2 ± 0.5	103.3 ± 1.8	92.6 ± 1.1	10.7	22-24	4.68 ± 0.55
DTI-04	106.4 ± 1.0	111.6 ± 0.6	93.6 ± 0.6	18	22-24	4.74 ± 0.30
DTI-05	105.0 ± 0.5	104.0 ± 1.0	89.6 ± 1.5	14.4	20-22	17.90 ± 3.81
DTI-07	100.0 ± 0.6	102.6 ± 1.5	78.8 ± 5.5	23.8	20-22	7.40 ± 2.97
DTI-08	111.2 ± 0.4	112.0 ± 1.0	89.6 ± 0.6	22.4	22-24	5.56 ± 1.27
DTI-22 ****	87.6 ± 1.0	88.8 ± 0.7	72.9 ± 0.7	15.9	32-34	3.05 ± 0.50
DTI-23	97.5 ± 0.9	-	-	-	22-24	9.60 ± 0.92
DTI-26	102.1 ± 0.6	104.5 ± 1.0	87.2 ± 2.6	17.3	22-24	1.10 ± 0.12
DTI-27	98.9 ± 1.0	102.9 ± 1.6	89.4 ± 5.1	13.5	22-24	4.86 ± 1.09
DTI-28	100.2 ± 5.8	108.9 ± 4.1	75.5 ± 5.6	33.5	22-24	9.14 ± 0.55
DTI-29	98.4 ± 2.3	110.2 ± 4.3	69.2 ± 3.7	40.9	22-24	10.60 ± 2.76
<i>DTI-Coatings (amphiphilic)*</i>						
DTI-09	109.5 ± 2.9	81.4 ± 4.7	0	81.4	***	5.66 ± 1.84
DTI-10	109.7 ± 1.8	90.2 ± 2.3	0	90.2	***	5.82 ± 1.04
DTI-11	109.5 ± 0.5	91.0 ± 1.2	28.6 ± 2.9	62.4	***	6.04 ± 2.02
DTI-24	~ 40	-	-	-	***	4.16 ± 1.50
DTI-25	81.2	-	-	-	***	3.20 ± 0.57
<i>ILAG coatings**</i>						
Coating	SCA [°] water	SCA [°] diiodomethene	SE (calculated) [mN m ⁻¹]	Thickness** [μm]		
ILAG-1	97.9	73.0	28.86	11.6		
ILAG-2	137.4	98.3	10.40	10.0		
ILAG-3	105.8	67.5	28.80	17.2		
ILAG-4	108.5	69.4	26.54	16.1		
ILAG-5	102.5	74.7	26.6	14.9		
ILAG-6	102.6	67.5	29.16	10.7		
ILAG-7	101.7	66.8	29.69	15.0		
ILAG-8	96.4	63.2	32.99	24.2		

* Measured at DTI.

** Measured at ILAG.

*** Not possible to measure the SE of the amphiphilic coatings with inks.

**** Sol-gel systems without repellent additive.

Table 2.1: water contact angles at room temperature and basic surface characterization of the tested coatings.

Coating ID	Type	Comment
12	Commercial	Silicone based marketed as icephobic coating (hydrophobic). Too thick for application on heat transfer surfaces (>100 microns)
13	Commercial	Silicone based marketed as fouling release (amphiphilic). Too thick for application on heat transfer surfaces (>100 microns)
14	Commercial	Epoxy protective coating (hydrophobic)

Table 2.2: Commercial coating included in the laboratory testing phase

2.2 BULK MATERIALS

The theory behind the bulk materials approach is based on the ice formation of the initial ice crystal. It is dated back to 1966 when Neville Horner Fletcher investigated the physics of rain clouds [3]. In clouds, the water droplets achieve a supercooling of $-40\text{ }^{\circ}\text{C}$ or even higher [4]. The high supercooling degree in clouds can be reached, since there are no other surfaces triggering the ice formation. If the freezing occurs with only water molecules, it is called homogeneous ice formation. When the freezing starts due to another surface, such as dust particles, it is called heterogeneous ice formation. This type of freezing typically starts at higher temperatures. This circumstance can be explained by the generally valid physical rule, according to which every process strives for the energetically most favorable state. When water is cooled below its freezing point at atmospheric pressure of $0\text{ }^{\circ}\text{C}$, it is energetically more favourable for the water molecules to form a crystal lattice. However, there is an energetic barrier which is called free surface energy. In this case, this energy describes the formation of a solid surface (ice crystal) in a liquid surrounding (water). The energies included can be described by the Gibbs equation [5]:

$$\Delta G = -\Delta G_V + \Delta G_S \quad (2.1)$$

Where ΔG is Change of free Gibbs energy, ΔG_V is the change of free volume energy and ΔG_S is the change of free surface energy.

Once enough supercooled water molecules striving to form a crystal lattice adhere to each other and cross the energy barrier of ΔG_S , the ice formation process starts. The retained energy described with $-\Delta G_V$ results in the rise of the supercooled water temperature up to the freezing point. As long as there are ice crystals present in the water, supercooling cannot be achieved. The molecules of the freezing water adhere to the existing crystal lattice. In a technical application, the surface of the heat exchanger material is always present and in contact with the water. The contact surface must be unfavourable for the water ice lattice. The atomic structure of the bulk materials used is amorphous, which means that it has no order, like a conventional glass. The idea is to introduce tensions in the near surface water caused by the amorphous "structure". In Figure 2.2, there is a mismatch of water molecules (light blue) to the base material (dark blue), resulting in displacement of the water molecules. These displacement is causing the tensions, which then increase the energy barrier to form the initial ice crystal, thus a higher supercooling can be achieved.

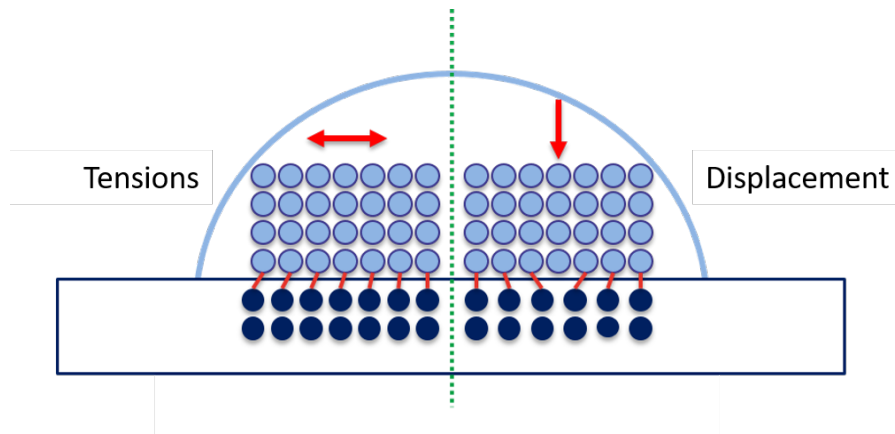


Figure 2.2: Tension within the water molecules due to a mismatch with the surface structure of the base material

Besides the freeze depression, it is important for the bulk materials to withstand the pressure in a compression refrigeration circuit. Moreover, the materials should have a high heat conductivity. Otherwise the supercooling layer will work as insulation in a heat exchanger increasing the needs of heat transfer area and thus of manufacturing costs. Even though the materials are designed for ice formation depression, freezing will sooner or later appear in the supercooler. In this case, the materials should not degrade so the supercooling performance becomes worse over time. Only a metallic approach was found to be suitable for these requirements. Amorphous metallic materials are already used as electric capacitors and are produced as thin band strip materials. They consist of different metal alloys such as iron, copper and aluminum. To form amorphous surfaces when the melt solidifies the materials also contain glass formers such as nickel, silicon and niobium. Since the atomic structure is amorphous it was assumed that iron is not likely to oxidize when exposed to water. A variety of twelve amorphous alloys were tested to show the surface structure influence. After the supercooling potentials of the alloys were tested, it was found that nickel-containing band strip materials show the most promising freeze depression and freeze delay. It was then decided to take a high phosphorous nickel treatment into account, since the application in an existing brazed plate heat exchanger is much easier than the band strip materials. It also forms an amorphous surface and fulfills the mentioned requirements. The composition of the tested materials are shown in Table 2.3.

Table 2.3: List of bulk materials

Name	Structure	Transition metal	Glass former	Trace metals
VIT 105	amorphous	Zirconium	Nickel, Copper	Titanium, Aluminium
AMZ 4	amorphous	Zirconium	Copper	Niobium, Aluminium
VZ 2106	amorphous	Nickel, Iron	Chromium, Silicon	Molybdenum, Boron, Copper
VZ 2133	amorphous	Nickel	Silicon, Boron	-
VZ 2170	amorphous	Nickel	Chromium, Phosphorous	Boron, Silicon
VZ 2255	amorphous	Copper	Tin, Nickel, Phosphorous	Zinc
VC 6025 G40	amorphous	Cobalt	Silicon, Iron	Molybdenum, Boron
VC 6025 I50X	amorphous	Cobalt	Molybdenum	Iron

Name	Structure	Transition metal	Glass former	Trace metals
VC 6030 D30	amorphous	Cobalt	Silicon, Iron	Manganese, Molybdenum, Boron
VC 7600	amorphous	Iron	Nickel	Boron, Silicon
VP 220	nano-crystalline	Iron	Nickel, Copper, Silicon, Niobium	Boron, Copper
VP 800	nano-crystalline	Iron	Silicon, Niobium	Copper, Boron
chem. Nickel	amorphous	Nickel	Phosphor	-

3 SMALL SCALE LABORATORY TESTING

In this chapter, an overview of the test methods and results for small scale lab testing, will be given. Based on these results, a selection of coatings and materials was carried out to be tested at large scale testing.

3.1 COATINGS: LABORATORY TESTS

Besides classical coating characterization techniques such as adhesion according to ISO 2409 and surface energy and wettability characterization, other more specific tests to evaluate the icephobic properties of coatings such as freeze depression and ice adhesion were conducted.

3.1.0.1 Freeze depression and freezing delay under atmospheric conditions

To carry out these measurements DTI used a proprietary test chamber. Where a cooling block cools either uncoated or coated plates. The contact area between sample plate and cooling block consists of a central Copper block, a plastic isolation ring made of POM (polyoxymethylene) and an Aluminium ring touching the outer edge of the plate. A peltier element is cooling the copper block, a PT 1000 thermocouple is measuring the copper block temperature. The contact between the copper block and the sample plate is through a thin, continuous ice film. A heating wire is heating the about 5 mm wide Aluminium ring. The contact between the Al-ring and the sample plate is by direct contact or through a minimal air gap of max. 0.1 mm. The heating of the sample edges is necessary to prevent contact freezing of the sample plate through contact with the edges and the ice between the plate's backside and the copper block. It is also important because ice is especially prone to form on the edge because of the specific geometric singularity and lower energy barrier for heterogeneous nucleation on this location.

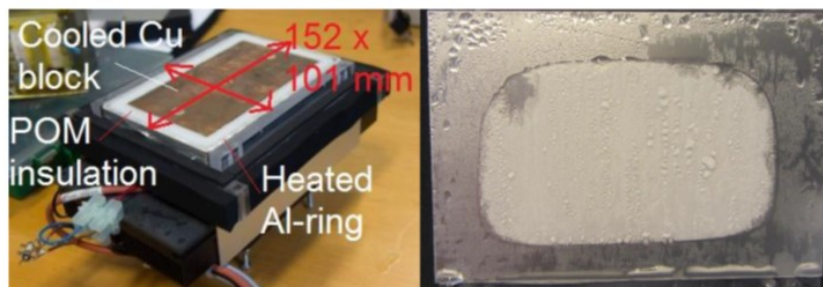
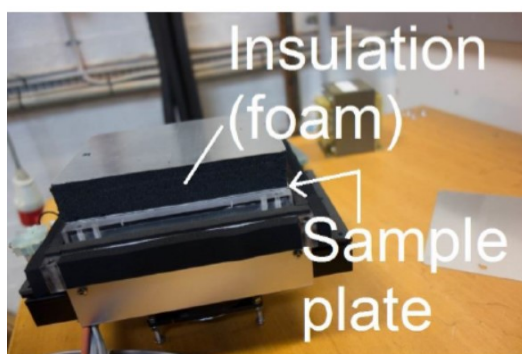


Figure 3.1: Detail of the DTI automatized set-up to measure the dynamic and static contact angle.

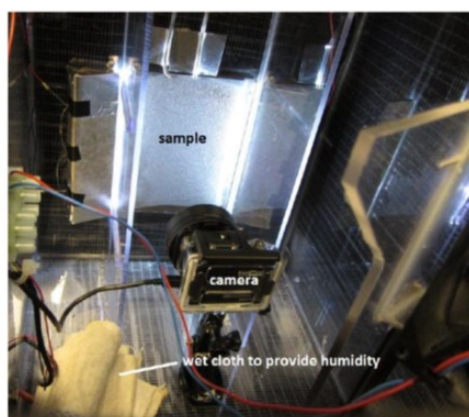
To start each test run, the sample plates (0.25 mm Al plates) were frozen to the Copper block. A water film was placed on the block, but not on the Al heating ring. The sample plate was placed on the water film. Edge heating power was adjusted to maintain a temperature just over 0 °C on the edges.



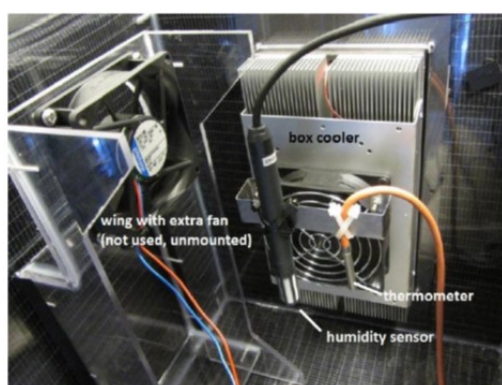
(a) Freezing the test sample to the cooling plate.



(b) The test box with a mounted plate on the left side.



(c) Inside of the test box. Front side with the sample plate and the camera. The cooling block is hidden behind the sample plate. A wet cloth is placed inside the test box to provide constant humidity.



(d) Inside of the test box. Back side with box cooler and temperature and humidity sensor.

Figure 3.2: Set-up for measuring the freeze depression and freezing delay in non-immersed conditions.

Freeze depression tests: After condensation, the plates were cooled by a rate of $0.1\text{ }^{\circ}\text{C}/\text{min}$. The temperature when the first occurrence of frost was observed, is regarded as the freezing temperature. The cooling was stopped at $-6.5\text{ }^{\circ}\text{C}$. However, if the sample was still ice free, it was hold at $-6.5\text{ }^{\circ}\text{C}$ for additional 1h. The coatings were tested at least 5 times.

Freezing delay: Additionally, the best performing coatings were tested to evaluate the freezing delay. In those tests, the plates were cooled after condensation directly down to $-6.5\text{ }^{\circ}\text{C}$, and then, they were hold at $-6.5\text{ }^{\circ}\text{C}$ until the first occurrence of frost. If after 3 h (180 min) there is no ice the test is stopped. The coatings were tested 5 times, and a score of 1 was given every time the sample remained ice free for at least 3 h. The higher was the score the more efficient was the sample in delaying the ice formation.

3.1.0.2 Freeze depression in submerged conditions

As final laboratory screening tool, a special device was constructed to investigate the icing process underwater conditions with water movement. The testing device is a round box tank made of stainless steel and consists of two parts. In the lower part there is a cooling block (Peltier element and a thermocouple) that controls the temperature of the disc sample. The contact between the sample and the Peltier element is through a thermal pad. The top part is mounted over the lower part and fixed with bolts. Two identical open silicone sheets are placed on and under the sample disc to ensure a watertight fit around the exposed area. The whole set-up is thermally insulated by PU foam.

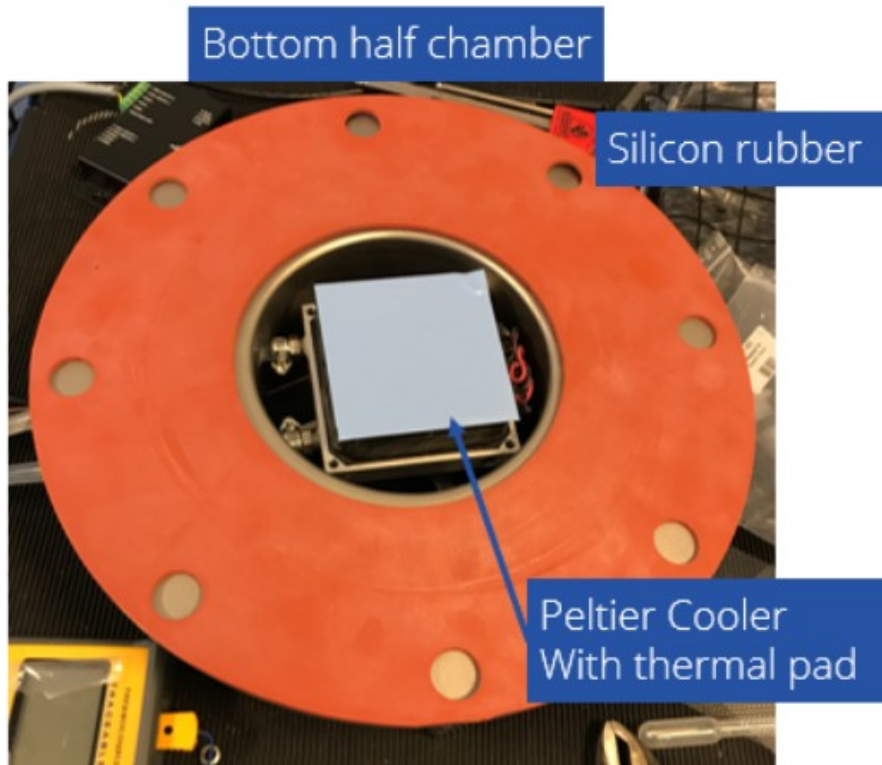


Figure 3.3: Detail of the lower part of the test set-up and ice detection system

A custom-made software with SpecView3 permits to control and monitor the cooling block temperature and the cooling rate, it is possible to record videos and pictures of the sample surface with 2 USB microscopes during the test. An external laboratory agitator served to introduce water movement.

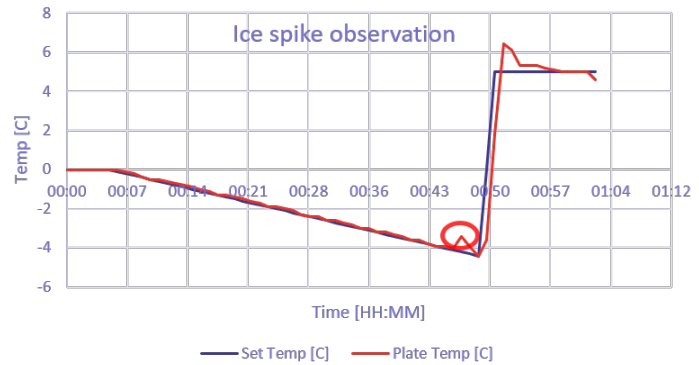
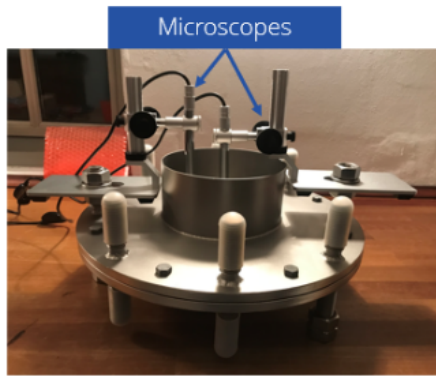


Figure 3.4: Left: Mounted test set-up for submerged icephobic testing. Right: Detection of temperature spike during ice formation.

For testing, the water tank is filled with 500 mL of demi water, the agitator is set to 150 rpm and the water tank is covered with a plastic lid with an opening for the agitator. The demi water is filled up to 1 cm below the plastic lid cover. The standard test procedure is computer controlled and it consist of the following steps:

1. The temperature in the water tank is set at 2 °C and is left for 2 h for tempering before starting the test.
2. After 2 h, the cooling rate is set at 3 °C/h and the cooling only stops once ice is formed or after reaching -15 °C. The computer detects the freezing by a temperature jump to the melting temperature, see right plot of Fig. 3.4.
3. After freezing occurs, the temperature is raised to 2 °C and it is held for 1.5 h, before the next cooling cycle begins.
4. A typical test consists of 5 consecutive cycles of freezing and melting.

3.1.1 Results and Discussion

3.1.1.1 Freeze depression under atmospheric conditions

For the first set of coatings, the screening process at small scale started with the freeze depression tests under atmospheric conditions.

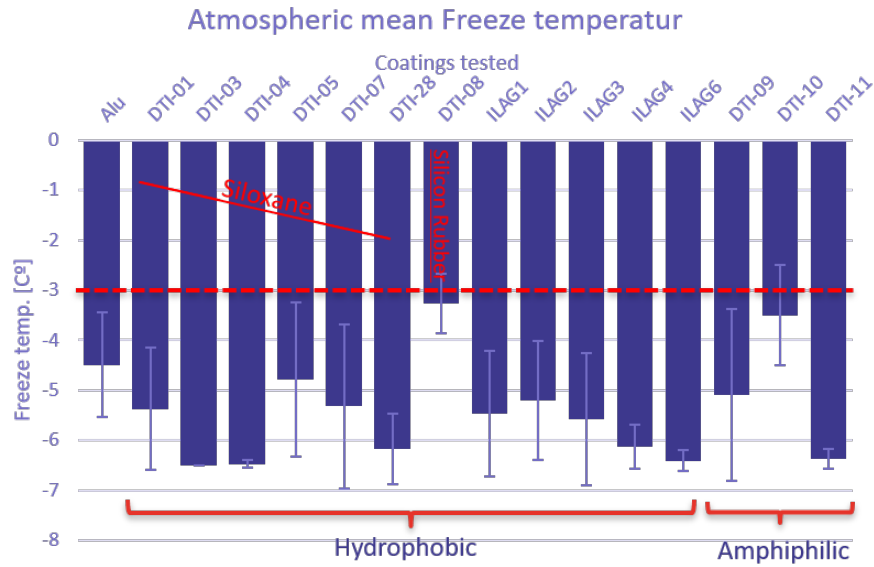


Figure 3.5: Freeze depression results. The standard deviation represent the variation n freezing points. The red line indicates the surface condensation temperature. DTI-03 reached maximum freeze depression in all tests.

Both hydrophobic and amphiphilic coatings have good candidates for freeze depression, where the most promising are DTI-03, DTI-04, ILAG-6 and DTI-11. Also there were high variety of results among the siloxane coatings, indicating that more than just hydrophobicity and chemical family has influence. To further narrow down the candidates, all coating which reached a temperate below -6°C was tested in the freeze delay test.

3.1.1.2 Freezing delay under atmospheric conditions

For the subsequent set of TRI-HP coatings, the screening at small laboratory-scale started with the freezing delay tests at -6.5°C . Table 3.1 displays the freeze depression data.

Material	Freezing delay score*	SCA[°]	RCA [°]	CAH [°]	Surface energy [mN m ⁻¹]
Aluminum Al 8006	0	92.6 ± 1.5	55.8 ± 3.1	36.6	58-60
<i>hydrophobic coatings</i>					
DTI-03	4	104.2 ± 0.5	92.6 ± 1.1	10.7	22-24
DTI-04	4	106.4 ± 1.0	93.6 ± 0.6	18	22-24
DTI-22**	2	87.6 ± 1.0	72.9 ± 0.7	15.9	32-34
DTI-23	4	97.45 ± 0.85	-	-	22-24
DTI-26	5	102.1 ± 0.6	87.2 ± 2.6	17.3	22-24
DTI-27	4	98.9 ± 1.0	89.4 ± 5.1	13.5	22-24
DTI-28	5	100.2 ± 5.8	75.5 ± 5.6	33.5	22-24
DTI-29	3	98.4 ± 2.3	69.2 ± 3.7	40.9	22-24
ILAG-4	1	108.5	-	-	26.5
ILAG-5	2	102.5	-	-	26.6
ILAG-6	5	102.6	75.4 ± 4.3	30.4	29.16
ILAG-7	3	101.7	-	-	29.69
ILAG-8	2	96.4	-	-	32.99
<i>Amphiphilic coatings</i>					
DTI-11	0	109.5 ± 0.5	28.6 ± 2.9	62.4	-
DTI-24	3	~40	-	-	-
DTI-25	2	81.2	-	-	-

Table 3.1: Data from freeze delay, freeze depression tests and contact angle analysis. Bolted coatings are the best performing ones with scores of 4 and 5.

*Samples score from 0 (Best) to 5 (Worst).

**Variant of DTI-3 with no hydrophobic additive.

From the reported data in Table 3.1 the following observations could be made:

1. Give the classically assumed stochastic nature of the freezing process, multiple tests are needed to determine if a coating has a real and statistically significant effect on the freezing process of water. A minimum of 5 tests were carried out for each sample. However, this might not be enough to get reliable data.
2. The best performing coatings (scoring 5) were DTI-26, DTI-28 and ILAG-6, followed by DTI-03, DTI-04, DTI-23, DTI-27 (scoring 4). Data did not permit to extract clear conclusions among specific surface properties and their effect on the freezing process. However, clearly the hydrophobic coatings outperformed the uncoated reference and the amphiphilic systems. Amphiphilic systems appears to have decreased efficiency when tested over a longer period of time, while the hydrophobic coatings retains their efficiency both in freeze depression and freeze delay.

The difference in test method between freeze delay and freeze depression, is a combination of the limitation of the test equipment and the environment. Freeze depression could, with better equipment, better determine differences between the best performing coatings. Since the test is stopped directly after the first ice detection, there the ice only interacts with a small part of the surface and there would be very little degradation due to ice formation. In

freeze delay test, due to test circumstances, the full surface is covered with ice before the test is stopped. This means that ice could have a much higher changes of degrading the surface due to ice formation. This could also be the reason that the amphiphilic coatings does not perform well in this test, but better in freeze depression. Ideally, the freeze depression test would be best, but in this case we find the overall best results with the freeze delay test because we also observe the degradation from ice formation. In future tests it would be relevant to observe changes in surface performance related to degradation by ice as well.

Based on the results from the freeze delay and freeze depression tests, the best performing coatings were tested in the submerge freeze depression. The idea is to analyse if there are any differences in the freezing trend from atmospheric to submerge freeze depression.

3.1.1.3 Ice adhesion

Results of ice adhesion of several samples are presented in Fig. 3.6. Both amphiphilic and most hydrophobic coatings showed low ice adhesion. Interestingly, ice adhesion results showed that amphiphilic coatings, both commercial and newly developed, showed extraordinarily low ice adhesion values. They are in the range of 15-20 kPa, and the reduction in the ice adhesion values compared to uncoated surfaces is higher than 95%. The good properties of amphiphilic coatings to lower the ice adhesion have been previously reported in the bibliography [6]. Accordingly, the hydrophilic component on the coated surface is capable of strongly binding the hydrogen molecules from the water, preventing the water from freezing at the surface. This forms a nonfrozen quasi-liquid layer that serve as self-lubricating interfacial liquid-like layer and helps to reduce the adhesion strength of ice to the surface.

The low ice adhesion could be a tool for easy ice removal inside the supercooler, if the massflow was increased sufficiently, but tests both elevated temperatures and during freeze delay showed that the stability of the amphiphilic coatings was not sufficient. For this method to be viable, more research into stable amphiphilic coatings is needed.

There are no clear connection between freeze depression and ice adhesion. The hydrophobic siloxanes seem to have both good freeze depression and low ice adhesion, but ILAG coating with good freeze depression does not necessarily have low ice adhesion.

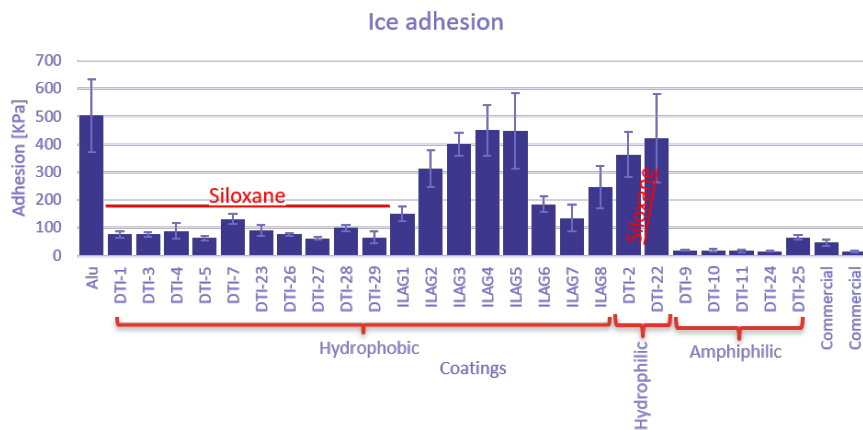


Figure 3.6: Results from share stress ice adhesion.

3.1.1.4 Submerged Freeze depression

The best performing coatings from the ice depression and ice delay test were submitted to the submerged ice depression test. The recorded data is presented in Table 3.7.

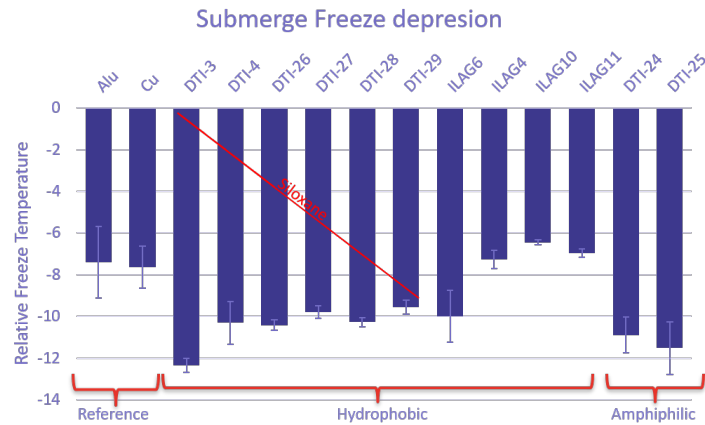


Figure 3.7: Freezing temperatures underwater (rpm 60, cooling rate 3 °C/h).

All coatings regardless whether they were hydrophobic or amphiphilic showed better performance than uncoated references. Coatings lowered the freezing temperature >3 K compared to uncoated references, and DTI-03 clearly outperform the rest of tested coatings. It is important to note, that the temperature from submerged freezing can not be directly compared with temperature from atmospheric freezing. Only the trend between the coatings can be compared.

When comparing results from atmospheric freezing and submergence freezing there are no clear trend between the coatings performance using the two different methods. When comparing hydrophobic and amphiphilic coatings in submerge conditions amphiphilic coatings showed better results, but additional tests revealed that they were less stable. In atmospheric conditions, hydrophobic coating showed the best results and higher stability. Since submerge freeze depression is nearest the conditions in the supercooler environment it makes sense to assume that this method would be optimal for further testing of freeze depression of new coatings. It appears that the degradation of amphiphilic coatings is not detected, which means that a specific testing method for ice related degradation may have to be investigated.

Classically, the freezing temperature has been correlated to the hydrophobic characteristics of surfaces [7, 8]. However, the TRI-HP results did not show any obvious link between the hydrophobic characteristics and the freezing temperature. The way solids promote ice nucleation is usually seen as the ability of surfaces to reduce the energy needed to build up the interface when an ice embryo develops. We believe that what rules the freezing temperature is the presence and density of active sites [9] for ice nucleation regardless the hydrophobic character of the surface. Therefore, the larger interface the more chances to find areas of high ice nucleation activity. Typically, grain boundaries and surface irregularities such as cracks and scratches are considered as locations for nucleation of ice. However, we acknowledge that we do not know the exact nature of the specific sites that contribute to ice nucleation and we cannot reproduce them. According to our hypothesis, any uniform and defect free surface is beneficial to lower the freezing temperature regardless its hydrophobicity, but factors such as surface morphology and changes in repellent additive may cause the difference between the coated surfaces.

It is important to remark, that the surfaces of metals used in industrial applications, certainly are less uniform and have much higher density of ice nucleating sites compared to laboratory surfaces. Therefore, extreme care should be taken when extrapolating results from laboratory research to practical macro-scale technologies with more non-uniform surface.

3.2 AMORPHOUS METALLIC MATERIALS: LABORATORY TESTS

The laboratory tests of the amorphous metallic materials include a basic screening of the supercooling potential. However, the screening method is already difficult to interpret because every parameter could affect the supercooling. For example the method by which the drop is deposited on the material or even vibrations of the experimental setup. This is why in the second small scale test the measurements took place in an insulated housing where the droplets were placed automatically. In this test a correlation between the moment of freezing and the free surface energy was analysed. For this purpose, the contact angle was measured constantly during a cooling process to detect any changes when the freezing process initiated. This section is intended to show the test procedure and the results as well as the conclusion for the following experiments with water flows.

3.2.1 Basic screening method

The preliminary investigation of the amorphous metallic materials supercooling performance is similar to the coatings. In a first attempt, the materials under investigation were placed on a cooling board. For better heat transfer, non-silicone heat transfer compound is placed between the amorphous material and the cooling plate. A defined deionized water droplet with 0.15 ml is placed on the center of the amorphous material by an adjustable pipette. Three temperature sensors are mounted on the surface of the material to be tested. To avoid contamination of the sample with undefined conditions from condensing water from the ambient air, the drop is tested in an enclosed environment. Fig. 3.8 shows a schematic layout of the test rig which combines a freeze depression and freeze delay tests.

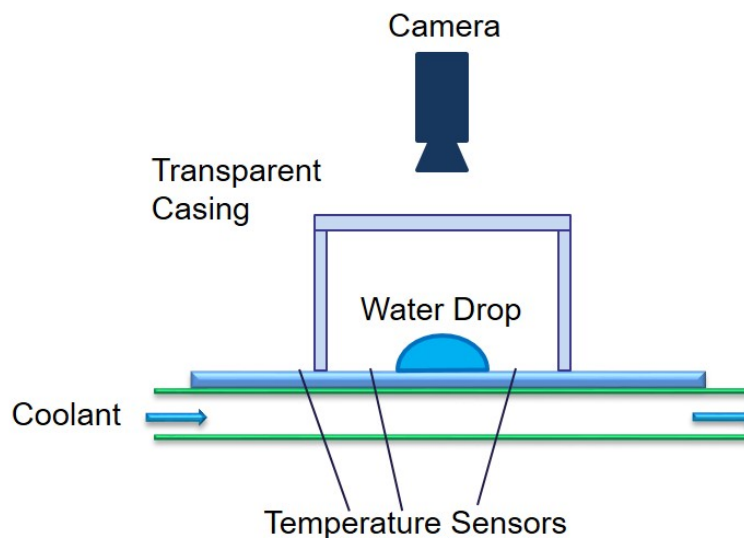


Figure 3.8: Schematic layout of the supercooling test rig.

The thermostat is preset at 1 °C. After the droplet is placed on the sample, the temperature of the thermostat is decreased to -11 °C. The cool down rate of the coolant is set to 5 K in 15 min and the cooling process of the droplet is monitored via a camera. If freezing is detected the temperature is recorded and the test is restarted. When the temperature of the thermostat reaches -11 °C, the holding time of two hours begins. Thus, this methods allows a combination of freeze depression and freeze delay testing. Each material is tested at least 5 times due to the stochastic character of freezing.

Results of using the combined freeze depression and freeze delay method for amorphous metallic materials are shown in Table 3.2, where Ra stands for the arithmetic average roughness value and Rz for the average peak-to-valley height. From the results presented, one can see that the amorphous metallic materials have a much a higher freeze depression and freeze delay potential than the reference materials copper and aluminum. The results confirm the increased supercooling potential of the tested amorphous metals. The temperature in Table 3.2 is either the average surface temperature when the droplet is freezing or the average surface temperature when the thermostat reached the lowest temperature and no freezing is detected. The column "avg. duration" shows the time after the lowest temperature has been reached without freezing. Besides the freeze depression, the surface roughness was measured by the key step method.

Table 3.2: Test results of freeze depression and freeze delay for metallic amorphous materials.

Material	Avg. freezing temperature	Avg. duration	Ra [μm]	Rz [μm]
Copper (Reference)	-7.6 °C	9 min	-	-
Aluminium (Reference)	-5.1 °C	0 min	-	-
Vitrovac 6025 I50X	-9.4 °C	115 min	0.395	1.992
VIT 105	-8.4 °C	120 min	0.171	1.971
AMZ 4	-8.6 °C	120 min	0.187	1.379

3.2.2 Advanced screening method

For the advanced screening method the supercooling test bench was implemented in a cooled housing. The air in the chamber was cooled down below the cooling plate temperature in order to minimize water from the air condensing on the sample. Furthermore, it was the attempt to find additional information on the exact event when water is rapidly forming an ice lattice. The theory explained in section 2.2 establishes the connection between surface free energy of the water on the contact material and the ice formation. This energy is usually measured by the sessile drop method described in DIN 55660-2:2011-12: "Determination of the free surface energy of solid surfaces by measuring the contact angle" [10]. For an ideal system (homogeneous materials and ideally smooth surfaces), the surface free energy ΔG_S is described in the Eq. 3.1, which corresponds to the equilibrium of forces in the horizontal direction:

$$\Delta G_S = \sigma_{LS} + \sigma_L \cdot \cos \theta_Y \quad (3.1)$$

Where θ_Y is the contact angle according to Young [11], ΔG_S is the free surface energy, σ_{LS} is the specific interfacial tension, and σ_L is the surface tension of the liquid.

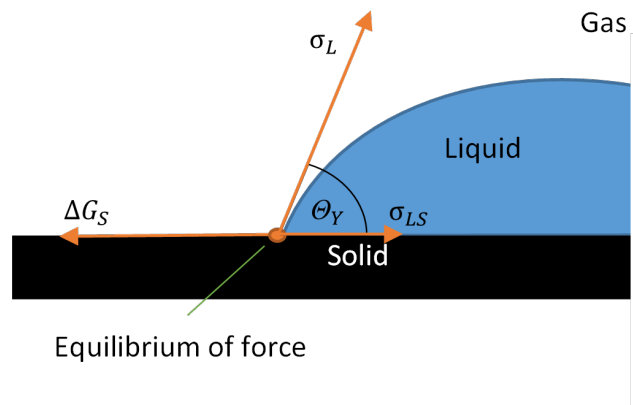


Figure 3.9: Equilibrium of force on contact angle according to Young [11].

To the authors knowledge, there was no investigation if the surface free energy of the water is changing when it is supercooled. It was the assumption that the water molecules will rearrange themselves to exceed the energy barrier. If the supercooled temperature is kept constant and the water only freezes afterwards, this process should be detectable by a changing contact angle. A digital microscope with a back light and an automated water drop placement has been installed in the test chamber. The constructed schematic layout is shown in Figure 3.10. A picture of the automated contact angle measuring unit with the cooling plate is shown in Fig. 3.11

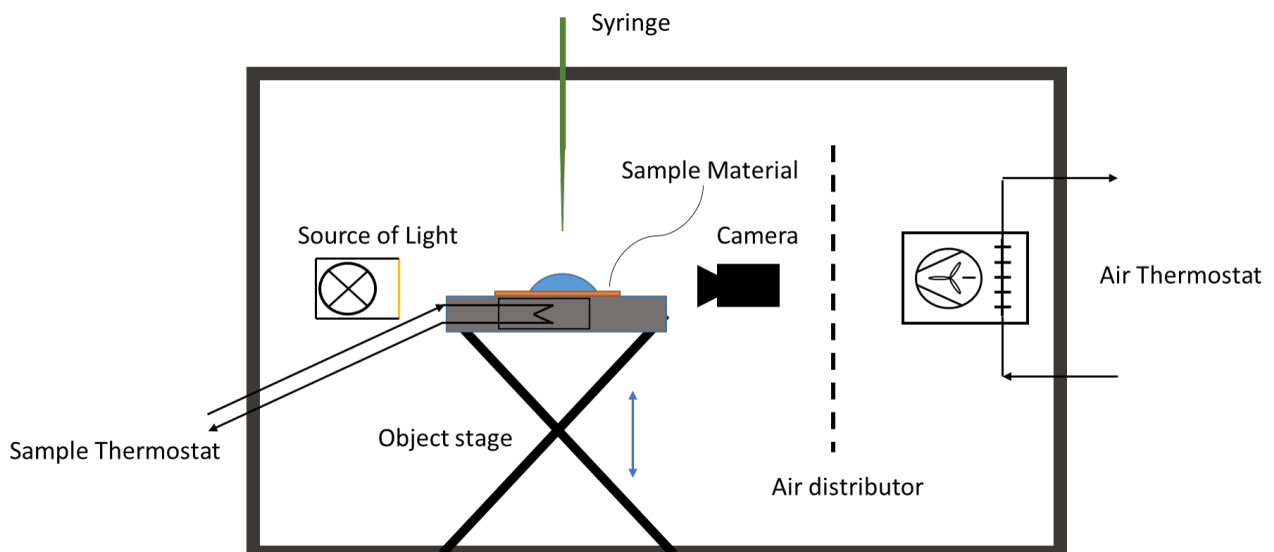


Figure 3.10: Schematic layout of the contact angle test rig.

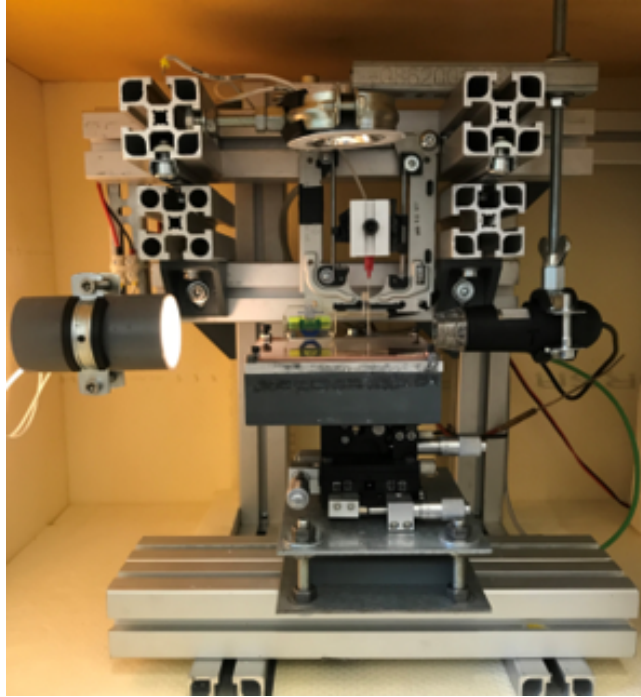


Figure 3.11: Developed experimental setup for supercooled contact angle measurement.

The supercooled contact angle measurement is performed in the thermally insulated housing. The object stage is cooled by a thermostat and the air inside the test rig is tempered by a second thermostat. By tempering the air the drop does not evaporate and at the same time the absolute humidity of the air is reduced avoiding condensation. For a contact angle measurement in a supercooled state, a tempered environment is essential, since condensate on the sample to be tested or evaporation would falsify the contact angles. An air distributor ensures that the cooled air is evenly distributed in the interior. The chamber and the stage are cooled to 1°C . The sample material is fixed on the stage with thermal paste. A $5\ \mu\text{L}$ large drop is created with the syringe. The stage is moved upwards to deposit the drop on the sample. The drop is moved with the stage to the center position of the camera and the first contact angle measurement is made. The temperature of the sample carrier is set to -10°C . The room cooling fans are turned off when the air temperature inside is below -10°C to minimize the air flow over the sample material and therefore the condensation on the surface. If the drop reaches -10°C without freezing, a second contact angle measurement is made. This condition is maintained for 60 minutes and the contact angle is observed during this time. If the drop freezes during cooling or holding or if the drop remains liquid after 60 minutes, the third contact angle measurement is initiated. Due to the aleatory phenomenon of ice formation, the measurement is performed three times for each sample.

The supercooled contact angle measurement allows to measure the three values in parallel: contact angle, supercooling and time freezing delay. Of particular interest are the measurements where maximum supercooling is reached and the drop freezes during the holding time. All amorphous metal alloys available as a band strip material were tested. An overview of the results is shown in Table 3.3.

Table 3.3: Test results of supercooled contact angle measurement.

Name	Freeze depression [°C]	Freeze delay [min]	Contact angle at 1°C [°]	Contact angle at -10°C [°]	Contact angle frozen [°]
Copper	-9.1	14	44.3 ± 3.4	44.2 ± 1.0	44.2 ± 7.0
Aluminum	-9.9	3	38.5 ± 9.5	41.0 ± 6.4	37.2 ± 9.0
VZ 2106*	-7.7	0	55.3 ± 2.9	-	52.9 ± 5.5
VZ 2133*	-10.0	37	36.2 ± 8.2	30.3 ± 9.9	30.5 ± 7.3
VZ 2170*	-10.0	27	46.6 ± 3.1	46.8 ± 3.1	47.5 ± 2.7
VZ 2255*	-10.0	18	35.0 ± 5.6	36.2 ± 6.8	33.7 ± 9.0
VC 6025 G40	-9.1	18	33.7 ± 1.5	32.8 ± 2.7	35.3 ± 3.0
VC 6025 I50X	-8.6	2	50.1 ± 7.4	59.0 ± 0.5	46.8 ± 7.1
VC 6030 D30	-7.7	0	62.1 ± 5.1	-	51.7 ± 5.2
VC 7600*	-9.0	40	46.6 ± 3.6	35.2 ± 2.6	42.3 ± 0.8
VP 220*	-10.0	29	57.9 ± 5.7	61.1 ± 3.4	54.9 ± 4.4
VP 800	-7.5	0	56.3 ± 9.8	-	53.4 ± 8.9

* Alloy contains nickel

Contact angle measurement during supercooling was performed to obtain additional information about the freezing process. This should establish a reliable method to evaluate the selection of the most suitable materials. However, the contact angle does not change, so no correlation between the supercooling potential and the contact angle can be found by the experimental setup. Therefore, the selection of the most promising materials are only based on the freeze depression and freeze delay.

From each group of the band strip material (Vitrobraze [VZ], Vitrovac [VC], Vitroperm [VP]) the most promising ones were used for the flowing water test setup. In case of the Vitrobraze material VZ 2170 was chosen instead of the VZ 2133 as it contains more abundant alloying elements. For commercial distribution, this would mean a lower price if the materials prove suitable. For the other material groups VC 7600 and VP220 were chosen for the upcoming tests. Compared within their material group the deepest freeze depression and the highest freeze delay were achieved with these materials. It should be noted that the materials with the most promising results all contain nickel as an alloying component. The free surface energy of these materials were tested by the OWRK method in the same test setup. To have a more information of the materials properties the advancing and receding contact angle at room temperature and supercooled at -5 °C were measured as well. The supercooled dynamic contact angle measurement required a hydrophobic cannula which is not touching the surface of the sample material. Otherwise, the cannula will start the ice formation as can be seen in Figure 3.12.

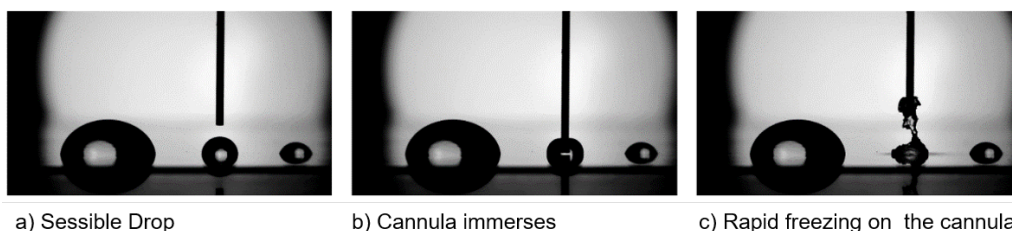
**Figure 3.12:** Cannula affecting the ice formation.

Table 3.4: Characterization of chosen metallic materials.

Name	Adv. CA [°]	Rec. CA [°]	Free surface energy [mN m ⁻¹]	Supercooled adv. CA [°]	Supercooled rec. CA [°]
Copper	73.2 ± 1.3	57.2 ± 1.8	41-42	-	-
VZ 2170	96.7 ± 2.1	72.4 ± 1.4	39-40	93.7 ± 1.9	57.5 ± 2.2
VC 7600	92.6 ± 0.8	24.9 ± 1.1	40-41	82.9 ± 2.3	33.6 ± 3.1
VP 220	92.5 ± 0.7	46.5 ± 1.5	40-41	82.9 ± 1.9	33.5 ± 2.5

3.2.3 Discussion

At first, it was necessary to confirm the theoretical approach of the amorphous metallic materials. The theory to achieve higher supercooling by introducing tensions in the near surface water was proved before on conventional glass tubes [12]. Nevertheless, it is mandatory to test the interaction of an amorphous metallic material with the water. In the basic screening method it was confirmed that the water on the these materials can be supercooled deeper and more reliable when compared with the untreated aluminum or copper. A closer investigation on the amorphous materials was carried out by measuring the contact angle when the water is supercooled. However, no correlation was found in the change of the contact angle of a frozen droplet.

The purpose of testing a variety of different alloys should exclude the influence of the alloying elements and underline the interaction between the surfaces atomic lattice and the surface near water. Anyhow, it appears that alloys containing nickel show a higher freeze depression and longer freeze delay. It is assumed that this alloying element retards the freezing process. The literature also shows that nickel forms an amorphous surface and is already used in the field of ice production [13]. After the tests it is still unclear if the amorphous lattice have the greatest impact on the supercooling. The surface free energy has not changed significantly compared to crystalline copper. It is expected that other factors affect the freezing process as well. Nevertheless, a high phosphorous nickel plating (electroless nickel) is therefore additionally considered as suitable for the upcoming large scale test with a water flow.

4 LARGE SCALE TESTING

In addition to the lab tests on sample scale the best performing coatings and bulk materials were selected to be tested on a larger scale under forced flow conditions to provide the next selection step before the heat exchanger supercooler test. Transferring experiments to a larger scale and using flowing water conditions leads to a more relevant view on the behaviour of different coatings as in a real heat exchanger. On a large scale, small defects in the coated surfaces are unavoidable and will effect the freezing preventing properties.

4.1 COATINGS: LARGE SCALE TESTING

4.1.1 Experimental test setup for coated tubes at SPF

Fig. 4.1 shows the setup of the tube test with flow conditions used at laboratory of SPF. The setup consists of two fluid cycles: i) the brine cycle flowing inside the coated pipe (orange) is cooled by a chiller and ii) the water cycle flowing in the annulus between the coated tube and the transparent PMMA pipe is cooled by the brine loop. The tube (coated pipe, yellow) is coated at the outer surface towards the water. Inside the tube there is a baffle plate (yellow wall inside the tube) to change the flow direction of the brine entering the tube via the lance (lance drawn black in the middle of the tube). For getting reliable and comparable results it is highly important to place the tube concentrically inside the PMMA pipe. Therefore, the distance between PMMA pipe and tube was fixed by three plastic screws (see Fig. 4.2) in the middle of the setup and close to the water inlet. Although soft plastic screws were used it was not possible to completely avoid any damage of the coating. The experiments should not be influenced by such damages as the location of the screws is 60 cm and 32 cm before the coldest point of the system where freezing starts. The transparent water tank as well as the tube-part were insulated during the experiments to avoid heat gains. The insulation was removable for getting a visual impression of where freezing was initiated and what was going on inside the tank (data of experiments without insulation were not used as valid data afterwards).

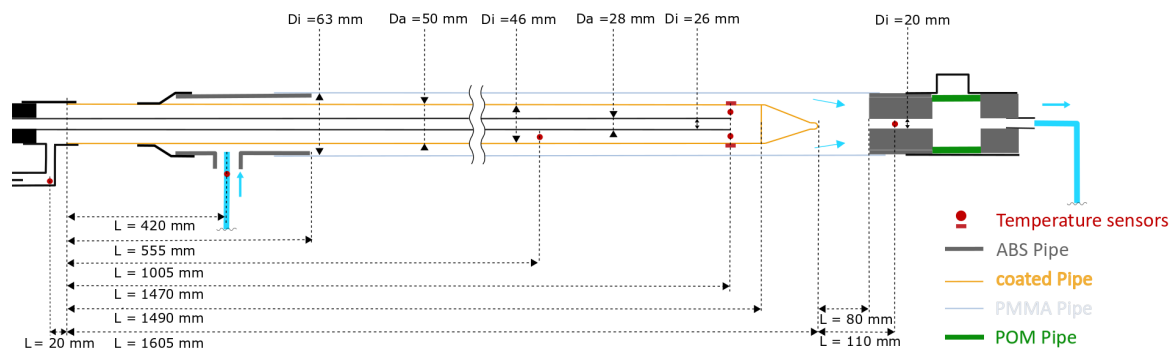


Figure 4.1: Setup of the tube test stand for copper tubes with numbers for the different temperature sensors. Black and blue arrows represent brine and water flows correspondingly.

The heat exchangers used in the residential heat pumps developed in TRI-HP are based on flat plates brazed with copper. Thus, the experiments were planned to be performed with a copper tube as base material. The tip of the tubes had to be welded to the tube. Welding copper appeared to be rather difficult and some tubes were not watertight at the welding seam. Therefore, later experiments have been performed with stainless steel tubes. The brine, which is cooled by a chiller, has a mass flow of approximately 2000 kg/h (slightly depending on the brine

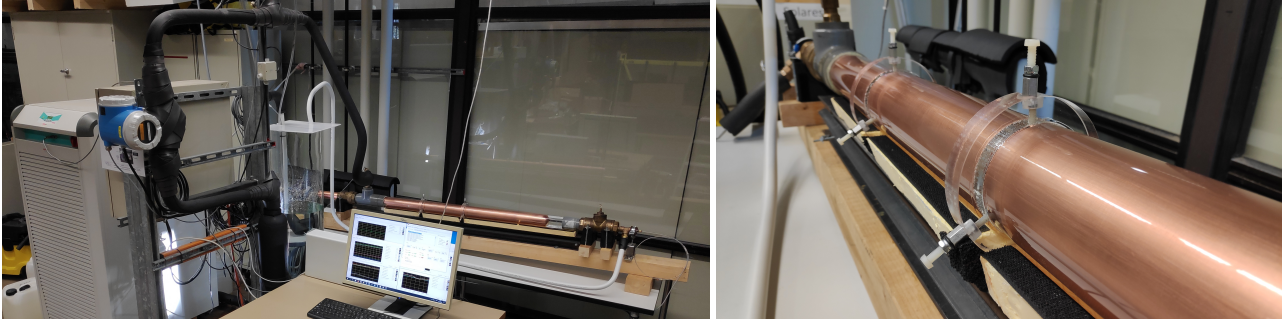


Figure 4.2: Test rig for testing coated tubes under flow conditions (left) and the copper tube within the transparent PMMA pipe with the plastic screws for fixing the concentric setting of tube and PMMA-pipe.

temperature). The red dots in Fig. 4.2 indicate the temperature sensors in the setup (described in Table 4.1). The brine enters the tube via a lance and changes its flow direction at the baffle plate inside the tube close to the welding seam. Therefore, the coldest region of the system is expected to be shortly before the baffle plate and the welding seam where the sensors 5 and 6 (for measuring $T_{tip,brine}$) are located. The temperature sensors number 7 and 8, indicated by a rectangle, are sensors for measuring the surface temperature in the coldest part of the system. As this temperature sensors are located in the water cycle at the part that has the coldest temperatures, they can influence the measurement by initiating crystallisation. Therefore, this measurements has been done with one tube (stainless steel tube, not coated) to validate a model for calculating the surface temperatures for the coated tubes afterwards.

Number	Description	Name
1	Inlet Temperature Brine	$T_{in,brine}$
2	Outlet Temperature Brine	$T_{out,brine}$
3	Inlet Temperature Water	$T_{in,wat}$
4	Mid Temperature Brine	$T_{mid,brine}$
5	Tip Temperature Brine (1)	$T_{tip1,brine}$
6	Tip Temperature Brine (2)	$T_{tip2,brine}$
7	Surface temperature of the water (1)	$T_{surf1,wat}$
8	Surface temperature of the water (2)	$T_{surf2,wat}$
9	Inlet Temperature Brine	$T_{out,wat}$

Table 4.1: Description of the temperature sensors used in the setup (See Fig. 4.2).

For each tube two experiments were performed with different mass flows in the water cycle, 1000 kg/h and 2000 kg/h. In each experiment, the water is cooled down gradually by decreasing the brine temperature in steps of 0.2 K. In each step, the brine temperature is kept constant for at least one hour to make sure that thermal equilibrium is reached and freezing is not initiated in this step. The average temperature of the last stable step (where no freezing occurs) is used as an indication for analyzing the ice preventing properties of the coatings. Freezing does not start at the same temperature in different cycles during one experiment as the freezing process is underlying statistical effects. The stable ice-free brine temperature (temperature at the last step before freezing starts) varies up to about 3 K within one experiment. At least six cooling cycles are performed for each experiment to get a reliable water freezing temperature and guarantee reproducible results. For the comparison of different coatings and not coated tube surfaces, the average value of the last stable steps for the tip, inlet and outlet temperature in the brine and inlet and outlet temperature in the water are used. The water temperature at the outlet and in the

tank are following the decreasing brine temperatures. The water inlet temperature ($T_{in,wat}$) is kept constant at a value of about 0.16 °C in order to prevent freezing of the water before entering the tube heat exchanger.

In order to compare the coatings in terms of their ability to allow supercooling of water the coated tube-water surface temperature at the coldest point of the setup had to be calculated. The heat transfer between brine and water is dependent on different factors:

- Material properties of the tube (and wall thickness).
- Fluid properties (especially thermal conductivity and viscosity) of the water.
- Fluid properties (especially thermal conductivity and viscosity) of the brine-water mixture, including changes in glycol concentration that were necessary during the different tests.
- Mass flow and resulting Reynolds Number in both fluids.

Covering all factors influencing the heat transfer and account for all the differences in the setting of the measurements we decided to perform CFD calculations using Open Foam® to get proper results. The geometry for both setups, with copper and stainless-steel tube, were meshed. The CFD calculation has been validated with experimental data of the measurements with surface temperature sensor in order to assume the correct heat gains from the surrounding (ambient air) and to make sure surface temperatures are calculated correctly. The thermal conductivity of the copper and stainless steel tube were assumed following the manufacturer's specifications (15 W/mK for the stainless steel tube, 393 W/mK for the copper tube). The thermal properties of the brine are adopted to the different brine concentrations and temperatures.

The mass flow measurement of the brine mass flow showed some uncertainties probably due to electrostatic charge by the fluid flow in a plastic pipe. The resulting uncertainty in the measurement was about 2.5 % of the mass flow rate. A change of 2.5 % in the brine mass flow rate results in a change of 0.6 % in the surface temperature. Additionally uncertainties in the temperature measurement of $T_{tip,brine}$ and $T_{in,wat}$ of 0.05 K each result in an error of the surface temperature of about 0.1 K. An additional error caused by uncertainties of thermal properties of the fluids is assumed to be about 2 % what leads to an overall relative uncertainty of the surface temperature about 4 %.

4.1.2 Results of tube tests with water flows

In Fig. 4.3 the brine temperatures at the tip of the tube for all experiments are shown. Experiments at 2000 kg/h were conducted before those at 1000 kg/h. For DTI-3 and ILAG-6 experiments the brine temperature of the last stable step increases with time, especially in the experiments with a flow rate of 1000 kg/h. This might be interpreted as a sign for aging or degradation of the coating and is further discussed later in this chapter.

In general the spreading of the temperature values of the last stable step within each experiment is up to 2.9 K (ILAG-6, mass flow of 2000 kg/h). The differences between different coatings and the stainless steel reference tube are much smaller than the spreading of the cycles within one experiment for a mass flow of 2000 kg/h in the water cycle.

For the experiments with lower mass flow of 1000 kg/h the spreading appears to be slightly less with a maximum of 2.6 K for the experiment with DTI-28. The differences between different coatings is larger with 2.5 K between the lowest (DTI-4) and the highest (ILAG-6) average freezing temperatures.

The comparison of the brine temperatures at the tip of the tube does not allow a fair comparison of the different coating properties. The differences in the experimental setting like different brine concentrations, copper and stainless steel tubes with different thermal properties and different wall thickness, influence the measured

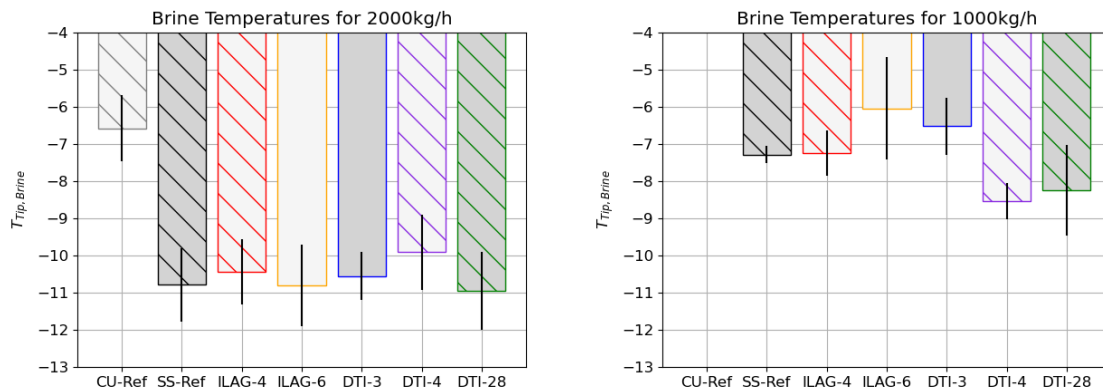


Figure 4.3: Overview about the brine-temperatures at the tip of the tube. The vertical lines indicate the variation of temperature measurements between different cycles, the bars show the average values of all cycles in one experiment. Dark gray indicates a stainless steel tube, bright gray a copper tube as base material. The not hatched bars indicate coatings that seemed to degrade during the experiment.

temperatures. By calculating the water temperature at the surface of the tube with considering these different parameters gives a surface temperatures that is not affected by all these changes. Fig. 4.4 shows the overview of the average surface temperature for each experiment calculated using the CFD with the available experimental data for each test. The differences between the different coatings are small for the experiments with a mass flow of 2000 kg/h. The differences between coatings with lower freezing temperature than the stainless steel reference tube (SS-Ref) are within the uncertainty of the measurement, but all coated tubes show a significantly lower freezing temperature at the surface of the tube than the copper reference tube. Therefore, every coating has the capability to improve a rough and/or defect surface like the one of the copper tube. In the experiments with a mass flow in the water cycle of 1000 kg/h. DTI-28 appears to improve the supercooling significantly by about 0.6 K compared to the stainless steel reference tube. Results of DTI-3 and ILAG-6, particularly at 1000 kg/h, should be taken with caution since these coatings seemed to degrade.

In the results of the experiments it looked like the freezing temperatures of DTI-3 and ILAG-6 coated tubes increased during time within the experiments, possibly due to aging or degradation of the coatings. A closer look shows some defects in both cases. Fig. 4.5 shows three defects within the coating ILAG-6 before and after the tube tests. The defects became green during the tests which might be a sign for oxidation or some other reaction which happened during or after the tests or due to parts of the coating being more porous or scratched.

4.1.3 Discussion

The copper reference tube shows a high roughness at the welding seam, the coldest region of the setup (Fig. 4.6). All coatings, even if not perfectly applied, show significant better results of the freezing temperatures than the copper reference tube. Thus, every coating seems to have a positive effect applied on a rough and/or defective surface by smoothing it.

However, coatings do not improve the freeze depression significantly compared to a stainless steel "defect-free" surface at high mass flows. It might be that the flow regime is either a dominant factor or it enhances surface

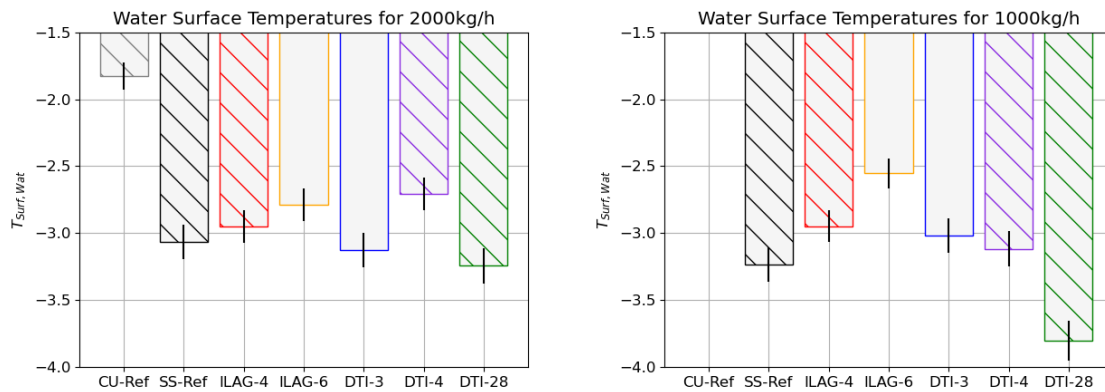


Figure 4.4: Overview about the Water-Temperatures at the surface of the tube at the coldest part of the water at the surface of the tube. The bars for the surface water temperatures of ILAG-6 and DTI-3 are marked with lines. These coatings seemed to degrade during the experiment. The vertical lines for each bar indicate the assumed resulting error on $T_{surf, wat}$ for each experiment. The not hatched bars indicate coatings that seemed to degraded during the experiment.

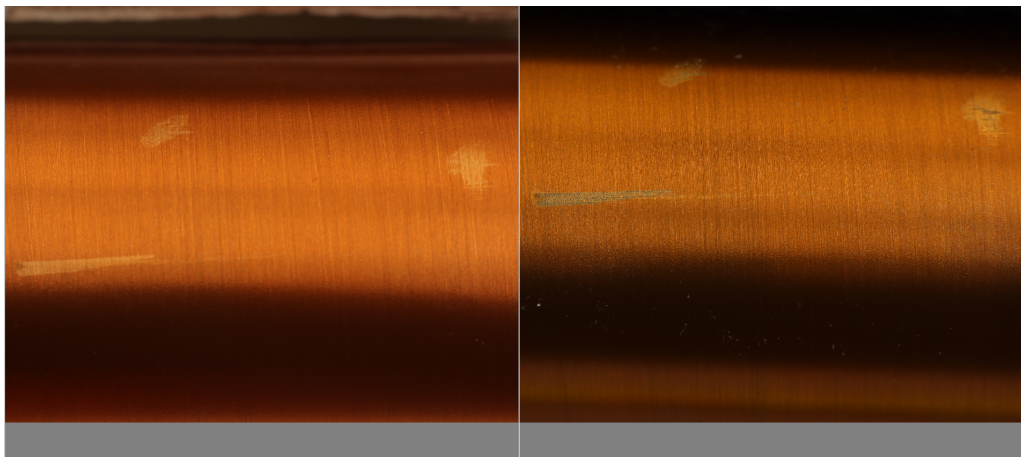


Figure 4.5: Part of the tube surface with ILAG-6 coating before (left) and after (right) the tube test at 1100 mm about 40 cm before the coldest point of the setup.

defects such that results are quite similar with all surfaces. As a consequence, a defect-free smooth surface might be a good solution with the advantage of being more durable than a coated surface.

The differences from all coatings were not large enough to decide which ones to use. Thus, it has been decided to test all these coatings in the brazed plate heat exchangers that will be tested in the power range of 5 kW. Results of the plate heat exchangers without a coating are expected to perform worse than the coated ones due to the non smooth surface found on typical copper brazed heat exchangers. Thus, it might be that a non-coated plate heat exchanger performs poorly, as the copper tube analysed on the tube experiments. Testing results of coated supercooler on the power range of 5 kW will be presented during spring of 2021.



Figure 4.6: Region around the welding seam for the copper reference tube. Several defects in and a rather rough surface are visible.

4.2 LARGE SCALE TESTING OF AMORPHOUS METALLIC SURFACES

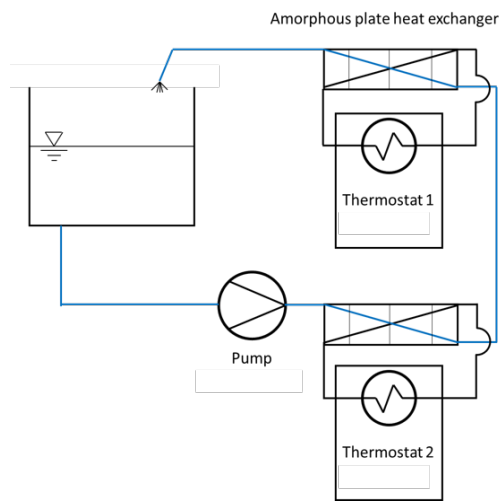
The large scale testing with water flows is intended to have similar operating conditions as the ones on the supercooled used on a heat pump system. A special tube-like heat exchanger was developed in order to test the most promising amorphous band strip metallic materials. The experimental heat exchanger was mounted in the test setup, where a cold brine was supercooling the water. In this setup, the water temperature was measured in the free jet. In all the amorphous metals selected, nickel was found to be present. Thus, it was considered to be a promising material for a surface treatment. An electroless high phosphorous nickel plating also creates an amorphous surface, while having a high heat conductivity and low ice adhesion. A coaxial tube with four fluid connected nickel treated tubes were installed in the experimental setup. This method is also feasible for brazed plate heat exchanger, which is why this procedure will be used for the following tests with the supercoolers.

4.2.1 Experimental setup at UASKA

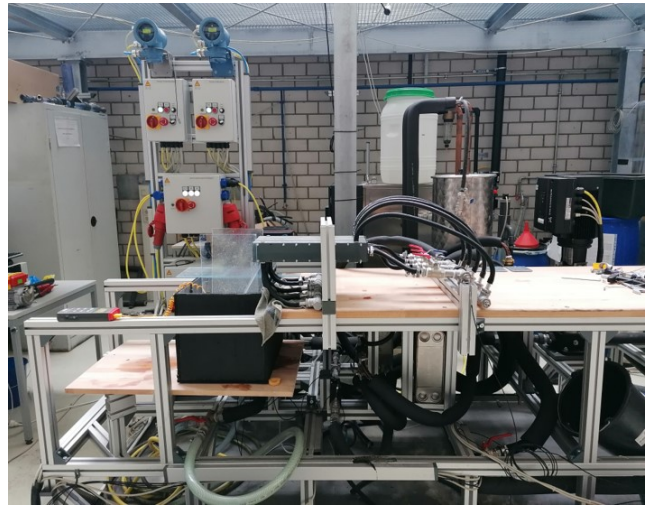
The experimental setup for testing the amorphous metallic materials includes two fluid cycles. Fig 4.7a shows a simplified version of the experimental setup. The primary cycle (blue) uses the pure water, while the secondary cycles contain a mixture of water with 20 % ethanol. The brine cycle replaces the propane or CO₂ refrigerant which simplifies the test setup and reduces manufacturing costs. The brine is cooled down to the set temperature by a chiller (Thermostat 1) before it flows through the experimental heat exchanger where the band strip materials have been applied. The temperature of the primary cycle with pure water is controlled by a second chiller (Thermostat 2). Thus, the water condition remains the same before it comes in contact with the experimental supercooler.

The outlet supercooled water from the tube-like heat exchanger flows as a free jet into a water tank. The temperature of the free jet is measured. This ensures that when the material of the temperature sensor acts as the nucleation side, the growing ice does not interrupt the measurement. Due to the impact of the splashing water ice is forming in the tank. Two pumps are controlled individually to adjust the flow regime and the temperature level. To achieve comparability, a mass flow of 300 kg/h is established for the experiments. For all tests, the brine temperature is set to -5 °C after the water in the buffer tank reached the start temperature of 1 °C. The outlet temperature is measured until the heat exchanger gets blocked by the freezing ice. With this test setup the real

conditions during supercooling in the evaporator are simulated. The water in the experiments is replaced every 24 h to reduce external contamination that might affect the outcome of the tests. A perforated plate in the tank and a filter before the primary pump also ensures the quality of the water.



(a) Simplified experimental setup



(b) Experimental setup in UASKA facilities materials

Figure 4.7: Amorphous materials experimental setup for flow tests.

For the metallic band strip amorphous material approach, a special tube-like heat exchanger has been developed in order to test the most promising materials selected from the static supercooling test presented in section 3.2. The aluminium base materials are milled into half-shells. Two half-shells mounted against each other creates an elliptical channel. The amorphous materials are placed inside the channels with heat conducting tape. The inlet adapter is designed with a conical edge to avoid the cutting edge coming into contact with the water. A CAD model of the supercooler and the assembly with the band strip materials are shown in Fig. 4.8 and Fig. 4.9

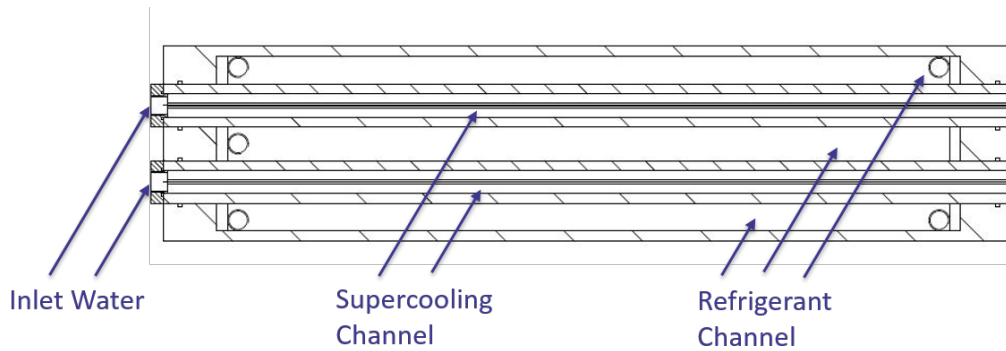
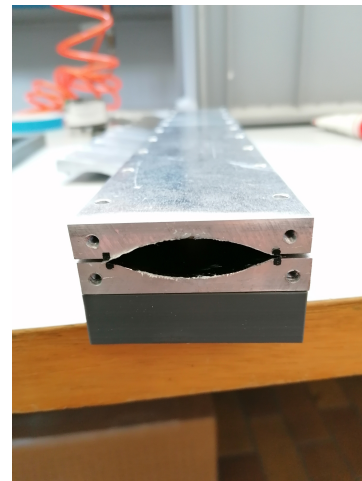


Figure 4.8: CAD- model of developed heat exchanger



(a) Application of the band strip materials materials



(b) Assembly of one channel

Figure 4.9: Experimental heat exchanger for band strip material testings

Besides the band strip materials, the ice depression performance of high phosphorous nickel treated tubes were compared with commercial available copper tubes. The 1 m long tubes have an inner diameter of 10 mm and are treated with the electroless high phosphorous nickel procedure. The pure water flows in the inner pipe. The brine flows in counterflow in the shell pipe and absorbs the heat to supercool the water. Four tubes are fluid-connected via hoses. In total, the experimental setup achieves a heat-transferring length of 3.6 m. A schematic layout of the tubes in shell supercooler is shown in Figure 4.10. The shell in tube heat exchanger is mounted in the same experimental setup and just replaces the band strip supercooler.

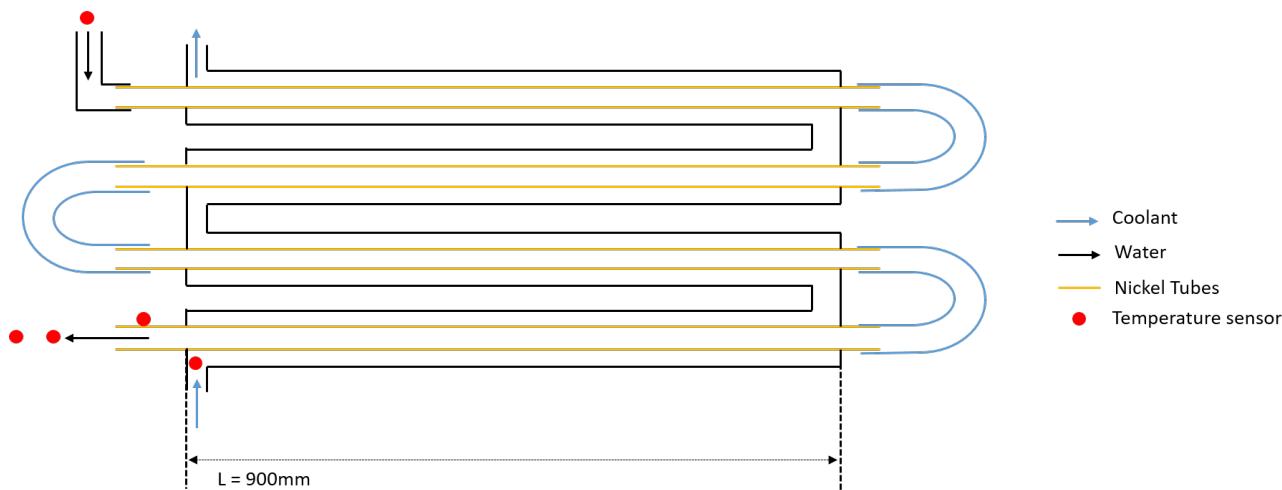


Figure 4.10: Simplified layout of nickel tube supercooler

4.2.2 Results of band strip materials

To compare the supercooling potential for a later application, the average supercooling over supercooled time from each run is taken as the validation parameters. Using average supercooling to calculate the heat exchangers power has the advantage that the heat exchanger operates at a temperature above its deepest temperature where supercooling is possible. The average supercooling is determined by calculating the average value of each data point below the freezing temperature:

$$T_{avg,x} = \frac{1}{n} \sum_{i=0}^n x_i \quad ; x_i \leq 0 \quad (4.1)$$

Data was recorded every two seconds for all tests. The band strip materials were tested in parallel in order to have a direct comparison of the best performing material in terms of supercooling. However, this way of testing had several issues. The blockage of one channel increased the mass flow in the other channels, thus decreasing the supercooling. This effect could be counteracted by readjusting the pump speed. But as soon as the growing ice at the first outlet reached another outlet the freezing was triggered in this channel. It was then decided to test each material individually.

The results are presented in Fig. 4.11 where each data point represent one test until freezing and the bar represent the average of all the data points. From this plot it can be seen that the VZ 2170 and VP 220 could be a potential candidate for a supercooler. However, since VP220 corroded only the VZ 2170 could be further considered. Moreover, the improvements respect to Aluminium were found to be small. Last but not least, the investigated band strip amorphous metal alloys are difficult to be applied in existing plate heat exchangers. As an alternative, a tube in shell heat exchanger, where these materials can be attached on the outside of the tubes, could be considered. However, the consortium agreed on using corrugated brazed plate heat exchanger because the higher efficiency and compact design. The use of a brazed plate heat exchanger is also reducing the refrigerant load which is important for the heat pump working with the flammable propane. In case of the CO₂, a tube in shell heat exchanger would need a high material strength to withstand the pressure that would increase the price significantly. By using a brazed plate heat exchanger, the thickness of the heat transfer plate is reduced, thus reducing thermal resistance and saving material and costs.

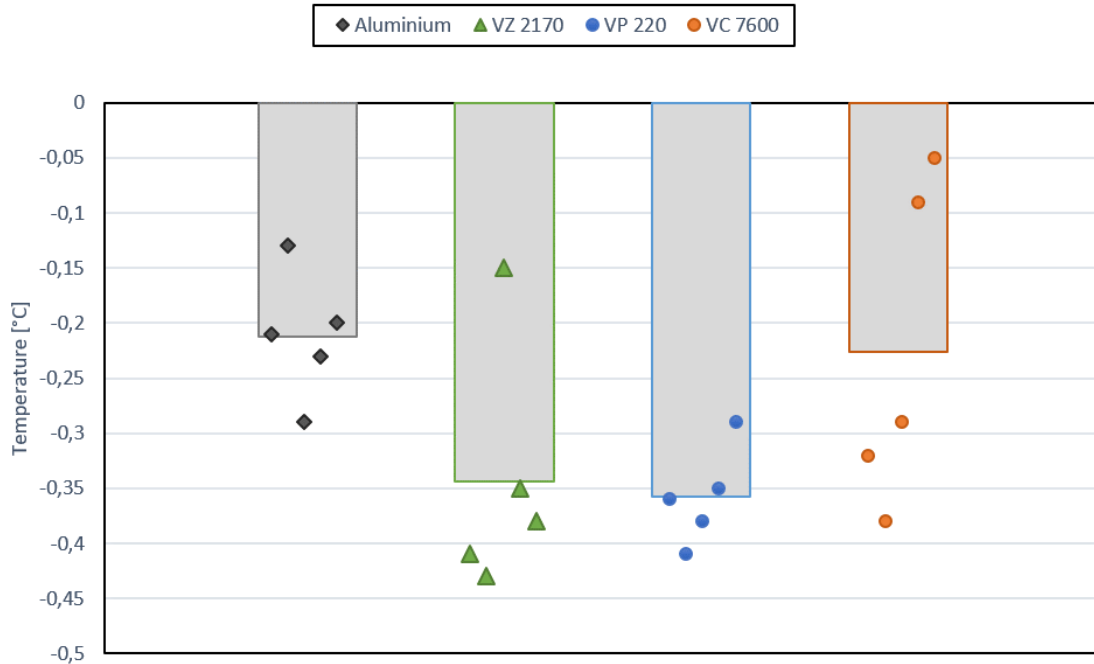


Figure 4.11: Results of the experimental tube-like heat exchanger with band strip materials.

In the previous static supercooling tests where water was in contact with the amorphous alloys for a few hours no corrosion could be detected (see Fig 4.12). According to literature, amorphous materials have a high resistance to rust because they have no grain boundaries in which oxygen atoms can perform the oxidation process [14]. Therefore, it was unexpected that some of the amorphous band strip materials show heavy corrosion after long term water exposure. It was then expected that the use of different metals in the primary water cycle lead to a galvanic corrosion which is why a separate corrosion test was carried out. The band strip materials were submerged completely in tap water and deionized water for a seven day period. The results are shown in Tab. 4.2. The corrosion of the material samples show the same results as the experimental heat exchanger. All alloys that that iron suffered from corrosion even that the alloys contained corrosion inhibiting components. The iron containing VP 220 have the alloying components niobium and nickel, which are known for their corrosion inhibiting effect [15]. On these samples partial corrosion can be detected. The VC 7600 also contains the corrosion inhabitant nickel but it appears to oxidize rapidly. Before the seven day period was over, the VC 7600 was already completely oxidized. For further applications only the VZ 2170, which contains no iron, is considered to be durable enough for the long term use. Due to all these reasons, the band strip materials will not longer be investigated within TRI-HP. On the electroless nickel treated tubes neither corrosion nor degradation was detected, which is why this approach will be used for the upcoming supercooler tests.

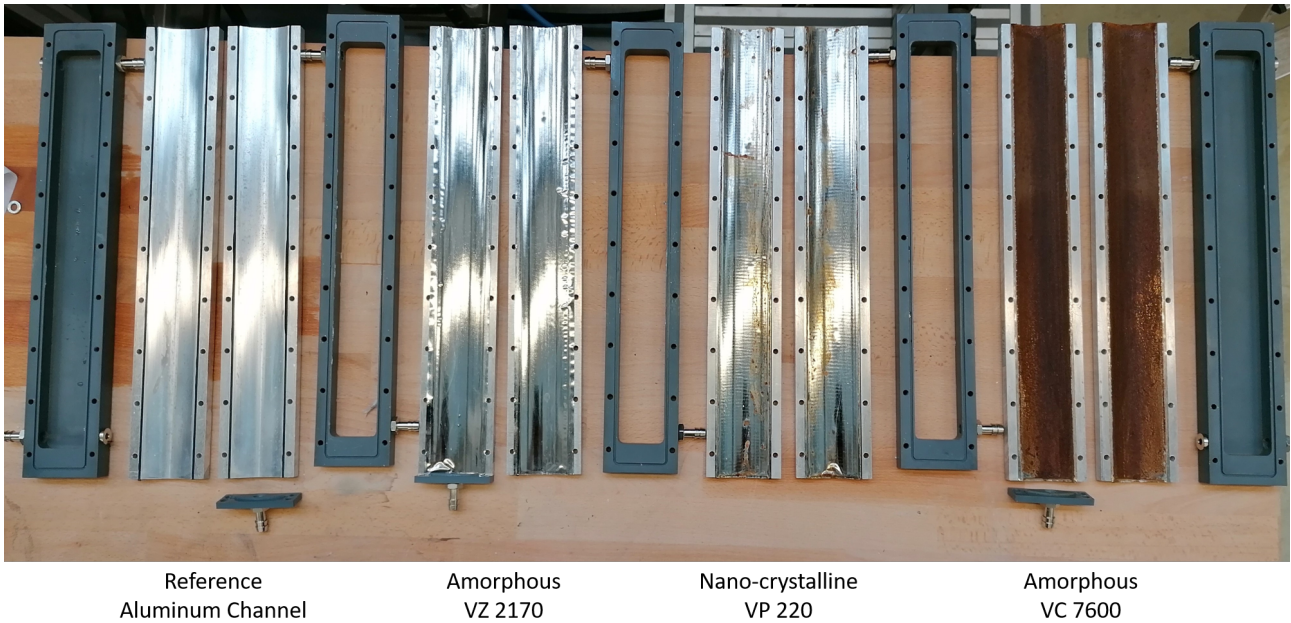


Figure 4.12: Disassembled experimental heat exchanger after long term water exposure

Table 4.2: Corrosion of the different amorphous alloys

	Transition metal	Glass former	Trace elements	Detected corrosion
Aluminum	Aluminum	-	-	none
VZ 2170	Nickel	Chromium, Phosphorous	Boron, Silicon	none
VP 220	Iron	Nickel, Copper, Silicon, Niobium	Boron	medium
VC 7600	Iron	Nickel	Boron, Silicon	heavy

4.2.3 Results of electroless nickel treated tubes

Besides the band strip material, the metallic approach of electroless nickel treated tubes was tested. A water mass flow of 300 kg/ h at a brine temperature of -5°C were also used in these experiments. The water temperature at the outlet of the tubes is monitored by two temperature sensors. Both of them are placed in the free jet before entering the water tank (see Fig 4.10).

Figure 4.13 shows the results of six tests with the copper tubes and the nickel tubes. In average the copper tubes are freezing soon at water temperature around -0.8°C . The nickel tubes appear to have beneficial properties with an average freezing temperature of around -1.4°C . The standard deviation of the tests also shows that the nickel tubes allow to supercool more reliable. The connecting hoses have not affected the outcome of the experiments. The blockage always occurred in the last tube where the temperature is the coldest. The 5 m long reference tube confirms that the connections did not affect the freezing. The results of the continuous copper are in the same range as the results with the separated copper tubes and are therefore not shown in the figure. The supercooled water forms sharp, arcicular ice crystals, which can become hooked and grow into an ice cone as it can be seen in Fig. 4.14. This must be detached manually during the experiments. Otherwise, it triggers the crystallization of the water as soon as it grows to the outlet.

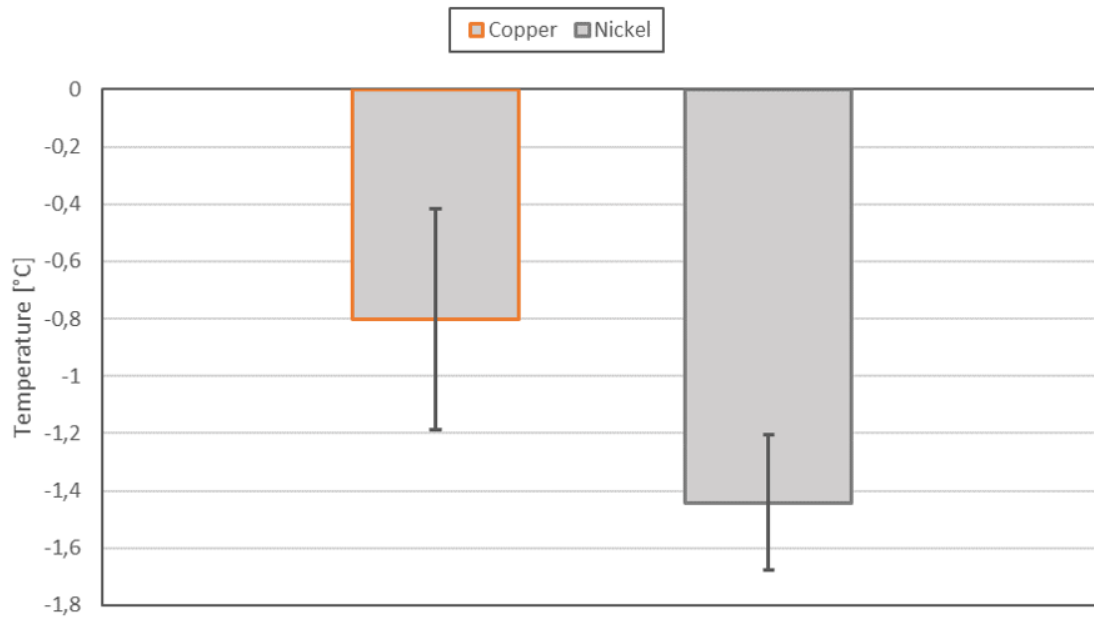


Figure 4.13: Results of tube tests with electroless nickel treated tubes.



(a) Ice growing upstream



(b) Acicular ice crystals

Figure 4.14: Supercooled water at $-1.5\text{ }^{\circ}\text{C}$ produced by high phosphorous chemical nickel treated stainless steel tube.

4.2.4 Conclusion

In the small scale tests with a static drop, a high supercooling was achieved on the band strip materials. Unfortunately, the same results did not occur when testing with a flow. Since the amorphous band strip materials are used in the field of electronics, there was no information on the effects of a long term water exposure. In the literature, amorphous materials are claimed to be resistant to corrosion, which has not been confirmed by experiments. All iron containing alloys have shown corrosion. Depending on the rare metals in the alloys, the band strip materials are furthermore costly. The materials can only be produced as band strips which makes it difficult to apply them in an existing heat exchanger. The use of these materials is no longer seen as feasible considering the cost and its difficult application on corrugated plate heat exchangers.

The path of band strip materials was not successful. However, this path lead to the new metallic approach of a electroless high phosphorous nickel treatment. This process also creates a smooth surface with an amorphous atomic structure. It is possible to pump the phosphor nickel through an existing heat exchanger covering up sharp edges and the braze joints. Electroless nickel is a common process used to protect the base material from corrosion, making it cost effective to apply to future supercoolers. The results of the nickel treated tube test already show a higher freeze depression compared to a copper tube. This amorphous metallic materials approach will be further pursued in the upcoming experiments of real supercoolers.

5 CONCLUSION

Within the activities on TRI-HP related to icephobicity, several different methods for assessing freeze depression and freeze delay for both coatings and metallic surfaces were developed and explored. Ten amorphous and two nanocrystalline materials and 26 coatings have been investigated in small scale surfaces with areas up to 25 cm² to identify the optimal surfaces. The aim was to select the best ones to be further analysed in large scale experiments with surfaces in the order of 0.3 m².

Coating strategies that were utilized were inorganic-organic hybrid coatings prepared from siloxanes, functionalized with organic precursors to achieve hydrophobic and amphiphilic surfaces and organic-inorganic with hydrophobic properties. The coatings were investigated by freezing at atmospheric conditions, submerged conditions and with ice-adhesion. These investigations showed that both amphiphilic and hydrophobic coatings had the ability to increase freeze depression by 1 K to 3 K compared to uncoated surfaces, in both submerge and atmospheric conditions, independent on surface energy and contact angle hysteresis. When comparing the chemical families, one would expect similar results from the same family, but results from the hydrophobic siloxanes showed that this was not the case. This means that other factors than the contact angle and surface energy could play a role in the anti-ice properties. A trend was that hydrophobic coatings had better long-term stability in water compared to the amphiphilic ones. The preferred strategy for further testing of coatings would be the submerged test method since the full surface is covered with liquid, thus the conditions are closer compared to a real supercooler. Coatings which perform good in atmospheric freeze depression conditions also perform good in submerge freeze depression. The main drawback of both submerge and atmospheric freeze depression is that it is more difficult to analyse coating degradation caused by icing. Based on the coatings that showed overall good results, five coatings were chosen to be further investigated in large scale testing with water flows.

Large scale testing with tube surfaces around 0.3 m² were used to assess which icephobic coating would perform better compared to non-coated ones in a more relevant environment with water flows. Coatings were tested with two water mass flows, i.e. 1000 kg/h and 2000 kg/h with water velocities of 0.24 m/s and 0.48 m/s respectively. Due to the low heat transfer rate of the tube heat exchanger, the supercooling degree was not a good indicator to assess the ice depression capabilities of different coatings. Instead, the coating-water surface temperature on the coldest spot of the tube, as recommended in [16], was used. Since it was not possible to directly measure the temperature on the surface, Computational Fluid Dynamics (CFD) calculations were used to take different heat transfer coefficients into account. Results show that for high mass flows there were very little differences on the coating-water surface temperature between all coatings and stainless steel. For lower mass flows one coating performed clearly better than the stainless steel. This indicates that coatings may have a bigger impact on lower flow velocities. It might be that the flow regime (turbulence) can have more influence than the anti-icing properties of the coatings. A relevant finding on tube experiments was that all coatings performed much better than a copper tube which had a rough/defective surface. Thus, it is expected that smooth coatings are likely to improve the performance of uncoated supercoolers, which are brazed with copper leading to a non-smooth and *defective* surface on the heat exchanger. The hypothesis is that any coating can cover those *defects* no matter how anti-icing will it be, which may mean that durability is more relevant than icephobicity when comparing smooth coatings. All these hypothesis will be further investigated in the supercooler test campaign using corrugated flat plates heat exchangers with a heat exchange power of around 5 kW.

The small scale test method of the amorphous metallic materials was based on the detection of the contact angle changes during the supercooling state and freezing process. However, it was found that the contact angle does not change during the freezing process. The reason for the sudden ice formation could not be observed, because it was difficult to avoid condensation or evaporation of the drop into the ambient air. Thus, a freeze depression

and freeze delay method applied on water droplets was used to select the best materials. Materials with best ice depression capabilities were found to contain nickel. From each material group, the best performing alloy was tested in the large scale experiments with surfaces around 0.04 m^2 with water flows. After a long term water exposure, the iron based materials showed heavy corrosion which was not expected, due to the pledged corrosion-preventing properties of amorphous structures. The poor supercooling performance and the difficult application of these band strip materials in a commercial available heat exchanger led to the decision of not pursuing this path any further. However, during this process it was found that nickel has advantageous properties. It can be applied like a coating, is corrosion resistant, durable and has an amorphous structure when a high phosphorous electroless plating method is used. Nickel tubes were investigated in the large scale test with surface areas around 0.13 m^2 and water velocities of 1.0 m/s . Results show a higher freeze depression when compared to copper tubes. Further experiments using corrugated flat plates of around 5 kW will be investigated in next steps.

BIBLIOGRAPHY

- [1] R. Losada, S. Holberg, J. Bennedsen, K. Kamuk, and F. Nielsen, "Coatings to prevent frost," *Journal of Coatings Technology and Research*, vol. 13, no. 4, pp. 645–653, Jun. 2016.
- [2] V. Upadhyay, T. Galhenage, D. Battocchi, and D. Webster, "Amphiphilic icephobic coatings," *Progress in Organic Coatings*, vol. 112, pp. 191 – 199, 2017. [Online]. Available: <http://www.sciencedirect.com/science/article/pii/S030094401730317X>
- [3] N. H. Fletcher, *The Physics of Rainclouds*. Cambridge University Press, 1966.
- [4] A. P. A.P. Khain, D. Rosenfeld, "Simulating convective clouds with sustained supercooled liquid water down to -37.5°C using a spectral microphysics model," *Geophysical Research Letters*, vol. 28, pp. 3887–3890, oct 2001. [Online]. Available: <https://doi.org/10.1029/2000GL012662>
- [5] G. Lock, *The Growth and Decay of Ice*. Cambridge University Press, 1990.
- [6] R. Dou, J. Chen, Y. Zhang, X. Wang, D. Cui, Y. Song, L. Jiang, and J. Wang, "Anti-icing coating with an aqueous lubricating layer," *ACS Applied Materials & Interfaces*, vol. 6, no. 10, pp. 6998–7003, 2014, PMID: 24828839. [Online]. Available: <https://doi.org/10.1021/am501252u>
- [7] H. Zhang, Y. Zhao, R. Lv, and C. Yang, "Freezing of sessile water droplet for various contact angles," *International Journal of Thermal Sciences*, vol. 101, pp. 59 – 67, 2016. [Online]. Available: <http://www.sciencedirect.com/science/article/pii/S1290072915003282>
- [8] F. Arianpour, M. Farzaneh, and S. Kulinich, "Hydrophobic and ice-retarding properties of doped silicone rubber coatings," *Applied Surface Science*, vol. 265, pp. 546 – 552, 2013. [Online]. Available: <http://www.sciencedirect.com/science/article/pii/S0169433212020004>
- [9] M. Holden, T. Whale, M. Tarn, D. O'Sullivan, R. Walshaw, B. Murray, F. Meldrum, and H. Christenson, "High-speed imaging of ice nucleation in water proves the existence of active sites," *Science Advances*, vol. 5, 12 2018.
- [10] "Paints and varnishes - Wettability - Part 2: Determination of the free surface energy of solid surfaces by measuring the contact angle," *Deutsche Industrie Norm*, 2011. [Online]. Available: <https://www.beuth.de/de/norm/din-55660-2/145842936>
- [11] T. Young, "An Essay on the Cohesion of Fluids," *Philosophical Transactions of the Royal Society*, pp. 65–87, december 1804. [Online]. Available: <https://royalsocietypublishing.org/doi/10.1098/rstl.1805.0005>
- [12] S. Gund and M. Kauffeld, "No Title," in *Experimental investigation on the supercooling effect of fluids confined in non-metallic vessels using pure water and silicon carbide*, Karlsruhe, Germany, 2019, p. 1.
- [13] K. P. Rolf Weiler, *Chapter 4: The properties of electroless Nickel*. American Electroplaters and Surface Finishers Society, 1990.
- [14] A. INOUE, "Stabilization of metallic supercooled amorphous alloys," *Acta Materialia*, vol. 48, pp. 279–306, jan 2000. [Online]. Available: [https://doi.org/10.1016/S1359-6454\(99\)00300-6](https://doi.org/10.1016/S1359-6454(99)00300-6)

- [15] E.-S. M. Sherif, "Effect of Nickel Content on the Corrosion Resistance of Iron-Nickel Alloys in Concentrated Hydrochloric Acid Pickling Solutions," *Advances in Materials Science and Engineering*, vol. 2017, pp. 1–8, may 2017. [Online]. Available: <https://doi.org/10.1155/2017/1893672>
- [16] D. Carbonell, D. Philippen, M. Dudita, J. Schmidli, M. Schubert, and K. Erb, *Slurry-Hp II - Development of a supercooling ice slurry heat pump concept for solar heating applications*. Institut für Solartechnik SPF for Swiss Federal Office of Energy (SFOE), Research Programme Heat Pumps and Refrigeration, CH-3003 Bern, 2020.



Trigeneration systems based on
heat pumps with natural refrigerants
and multiple renewable sources



This project has received funding from the European Union's Horizon 2020 research and innovation programme under grant agreement N. 814888. The sole responsibility for the content of this paper lies with the authors. It does not necessarily reflect the opinion of the European Commission (EC). The EC is not responsible for any use that may be made of the information it contains.

©TRI-HP PROJECT. All rights reserved.

Any duplication or use of objects such as diagrams in other electronic or printed publications is not permitted without the author's agreement.